POLITECNICO DI TORINO
Repository ISTITUZIONALE

Structural complexity as a new paradigm in construction cost optimization

Original
Structural complexity as a new paradigm in construction cost optimization / Ma, Y., Song, C., Sardone, L., Xiao, R., Marano, G.C.. - In: COMPUTER-AIDED CIVIL AND INFRASTRUCTURE ENGINEERING. - ISSN 1093-9687. - 51:(2026), pp. 1-19. [10.1016/j.cacaie.2026.100186]

Availability:
This version is available at: 11583/3014610 since: 2026-08-19T02:39:59Z

Publisher:
Elsevier

Published
DOI:10.1016/j.cacaie.2026.100186

Terms of use:

This article is made available under terms and conditions as specified in the corresponding bibliographic description in the repository

Publisher copyright

(Article begins on next page)

26 November 2026

Computer-Aided Civil and Infrastructure Engineering 51 (2026) 100186

Contents lists available at ScienceDirect

Computer-Aided Civil and Infrastructure Engineering

journal homepage: www.sciencedirect.com/journal/computer-aided-civil-and-infrastructure-engineering

Research Article

Structural complexity as a new paradigm in construction cost optimization

Yuan Ma [a, b], Chaolin Song [c, a, *], Laura Sardone [b], Rucheng Xiao [a], Giuseppe Carlo Marano [d, b]

[a] Department of Bridge Engineering, Tongji University, Shanghai, 200092, China
[b] Department of Structural, Geotechnical and Building Engineering, Politecnico di Torino, Torino, 10100, Italy
[c] Department of Civil Engineering, The University of Hong Kong, Hong Kong, China
[d] College of Civil Engineering and Architecture, Henan University of Technology, Zhengzhou, 450001, China

ARTICLE INFO

Keywords:
Parametric structural design
Structural complexity
Multi-objective optimization
Construction cost optimization

ABSTRACT

Structural optimization in engineering has traditionally focused on minimizing material weight to enhance efficiency and performance. However, due to fabrication, transportation, and assembly requirements, minimizing material consumption does not necessarily minimize total construction cost. Lightweight designs may involve increased nodal connectivity, a higher diversity of cross-sections, or the use of oversized or overweight members, thereby raising production effort, installation complexity, and logistical costs. To address this issue, three dimensionless indices are proposed in this study, namely typological complexity, nodal complexity, and logistical complexity. These indices enable a quantitative assessment of structural complexity to be performed alongside material weight. When embedded into a multi-objective optimization framework, they allow structural designs to be evaluated in terms of material efficiency, manufacturing standardization, topological simplicity, and logistical convenience. In this way, trade-offs among these competing design aspects can be systematically explored. The applicability of the proposed framework is demonstrated through three case studies: a planar cantilever truss, a three-dimensional geodesic dome, and an industrial steel building. The results show that the proposed indices can provide complementary information beyond material weight and enable a more comprehensive evaluation of alternative structural designs. Consequently, the framework supports more informed decision-making during early design stages.

1. Introduction

1.1. Background and motivation

The structural design process is commonly divided into three major stages: the conceptual design stage, the preliminary design stage, and the detailed design stage, as shown in Fig. 1. Among these, the conceptual design stage plays a dominant role, as it defines the fundamental structural scheme, including the global layout, load-transfer mechanisms, and primary member arrangement (Ma et al., 2026). This stage is characterized by a high degree of design freedom, ranging from general topology and geometry to member sizing. It allows substantial modifications to the structural system, and has a profound and long-lasting influence on fabrication, construction feasibility, and the total project cost (Evers & Maatje, 2000).

Structural design optimization aims to improve structural performance through systematic adjustments of design variables under prescribed constraints, with the goal of achieving safe and economical solutions. Structural optimization conducted at the conceptual design stage is particularly effective in influencing the economic performance of engineering structures, owing to its high flexibility in altering topology and geometry (An et al., 2025; Ruy et al., 2001; Zhang et al., 2023), as well as its decisive impact on downstream processes (Frangedaki et al., 2021). Traditionally, such early-stage optimization has primarily focused on minimizing material consumption, typically by minimizing weight or volume (Erbatur & Al-Hussainy, 1992). Weight-based objectives are attractive at this stage because they provide a simple and intuitive metric for comparing alternative structural schemes.

However, the total installed cost of an engineering structure is generally not a linear function of its material weight alone (Ashworth & Skitmore, 1983). Fabrication, assembly, transportation, and erection may contribute substantially to the overall cost (Ruby, 2008). This distinction is particularly important for steel structures. Unlike concrete structures, whose costs is often strongly influenced by concrete volume, reinforcement, and formwork-related expenses

* Corresponding author at: Department of Civil Engineering, The University of Hong Kong, Hong Kong, China.
Email addresses: 2011156@tongji.edu.cn (Y. Ma), songcl@tongji.edu.cn (C. Song), laura.sardone@polito.it (L. Sardone), xiaorc@tongji.edu.cn (R. Xiao), giuseppe.marano@polito.it (G.C. Marano).

https://doi.org/10.1016/j.cacaie.2026.100186
Received 28 April 2026; Received in revised form 1 August 2026; Accepted 11 August 2026
Available online 12 August 2026
1093-9687/© 2026 The Authors. Published by Elsevier Inc. This is an open access article under the CC BY license (http://creativecommons.org/licenses/by/4.0/).

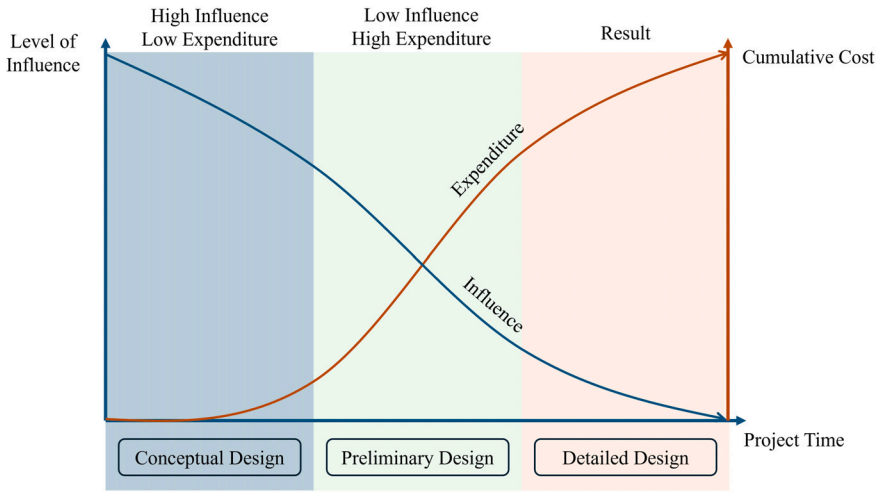

Fig. 1. Design stages.

(Sirca Jr & Adeli, 2005), steel structures are highly sensitive to fabrication complexity, cross-sectional diversity, joint detailing, and logistical requirements. Published benchmarks consistently support this observation. Fig. 2 reports that raw materials and fabrication each typically account for 30–40% of the cost of a steel frame, while on-site construction accounts for approximately 10–15%. Similarly, Carter and Schlafly (2008) emphasize that fabrication and erection labour constitute a substantial share of steel construction costs and that minimum weight does not necessarily correspond to minimum cost. This broader cost perspective is also adopted by Barg et al. (2018), who identify material, fabrication, and erection as the principal components of the total installed cost of structural steel frames. Vares et al. (2019) reported cost ranges of 600–750 £/t for raw materials, 325–455 £/t for fabrication, 120–167 £/t for construction, and 22–25 £/t for transportation of new structural steelwork. Although these proportions vary with structural type, location, market conditions, and project-specific factors (Rafiei & Adeli, 2018), they demonstrate that weight alone is insufficient to represent construction cost. In particular, cross-sectional diversity can increase procurement, fabrication, and inventory demands (De Biagi et al., 2024; Hayalioglu & Degertekin, 2005); complex nodes can increase detailing and assembly effort; and large or heavy members may require special transportation and lifting arrangements. These constructability-related characteristics may increase cost, duration, and execution risk even when a design is materially efficient (Arditi et al., 2002; Russell et al., 1994), while highly fragmented layouts may also compromise structural clarity and architectural coherence (Melchiorre et al., 2026).

Accordingly, this research aims to extend conventional material-based structural optimization frameworks by explicitly incorporating construction-related cost components associated with structural complexity, thereby providing a more realistic and practically relevant basis for early design stages.

1.2. Literature review

Traditional structural optimization formulations that focus exclusively on minimizing material consumption often produce designs with a wide variety of cross-sectional profiles, numerous nodes, and many small members (Melchiorre et al., 2025). This tendency is particularly evident in topology optimization (Dorn et al., 1964), where members are individually sized to reduce structural weight, and small members are generated to improve the load-transfer efficiency. Although such solutions may be materially efficient, their diverse sections and fragmented layouts can increase fabrication, connection, transportation, and erection efforts.

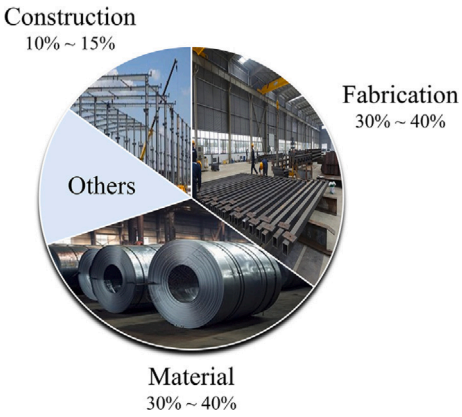

Fig. 2. Cost components of a typical steel frame (SteelConstruction.info, 2024).

Grouping is a widely adopted strategy for improving the practicality of optimized structures by assigning multiple members to common cross-sectional profiles. Groups have been defined according to internal forces (Krishnamoorthy et al., 2002), member lengths (Biedermann & Grierson, 1995), and sectional properties (van Woudenberg & van Der Meer, 2021; Walls & Elvin, 2010), while clustering techniques such as K-means have enabled more automated classification (Lu & Xie, 2023). For topology-optimized structures, grouping is often combined with post-processing or rationalization procedures. He and Gilbert (2015) simplified overly complex truss layouts by merging nearby nodes and modifying member intersections, while Lu and Xie (2023) combined clustering with geometry optimization. A similar strategy was subsequently applied to frame structures by Liu et al. (2023).

An alternative is to control complexity directly during optimization through additional objectives, constraints, or cost terms. Early studies introduced notional joint lengths (Parkes, 1975) or explicitly penalized the number of members and nodes (Torii et al., 2016). More recent formulations have considered the number of distinct profiles and member subdivisions (Cucuzza et al., 2024), connection costs (Asadpoure et al., 2015), and fabrication-related penalties (Lai et al., 2025). Multi-objective approaches have also been used to expose the trade-offs between structural weight and profile diversity (Carvalho et al., 2024; Melchiorre et al., 2025), constructability (Moroni & Forcael, 2026), and environmental or project-level performance (Peng et al., 2023). These studies demonstrate the value of Pareto-based decision-making, although

they generally consider only a limited subset of construction-related attributes.

The economic consequences of complexity also depend on the adopted manufacturing system. Modular production and robotic automation can reduce repetitive labour and production time, while requiring additional investment in machinery, programming, and maintenance (Ouda & Haggag, 2025). Additive manufacturing further changes the cost structure of complex connections. In particular, Wire-and-Arc Additive Manufacturing has been combined with structural optimization to produce complex steel joints that would be difficult to manufacture using conventional cutting and welding processes (Chen et al., 2024; Laghi et al., 2024). Such technologies may reduce the conventional penalty associated with nodal complexity, but introduce manufacturing time, deposition, post-processing, and inspection requirements. Complexity costs should therefore be regarded as dependent on the available fabrication technology.

Several studies have demonstrated how construction-related costs can be derived from measurable production information. Process-based steel cost models calculate material, cutting, welding, assembly, and erection costs from operation quantities and production rates (Pavlovčič et al., 2004). BIM-derived quantities and actual fabrication records have also been used to estimate shop labour requirements and fabrication costs (Hu et al., 2014; Mohsenijam & Lu, 2016). Barg et al. (2018) automatically generated fabrication-level bills of quantities from structural models and combined them with supplier unit rates to estimate material, fabrication, and erection costs during early design. These studies indicate that real project records, labour hours, supplier prices, and contractor quotations can provide a practical basis for identifying project-specific complexity parameters.

BIM provides an advanced information structure for linking structural geometry and detailing with quantities, schedules, and cost data. Recent studies have extended this capability through 5D BIM for integrated cost estimation and control (Pishdad & Onungwa, 2024), construction digital twins for incorporating site and production feedback (Saif et al., 2024), and machine-learning models that relate BIM features to recorded fabrication and assembly performance (Karadimos & Anthopoulos, 2024; Soh et al., 2022). These technologies support the identification and updating of project-specific cost and productivity relationships, although the resulting models remain dependent on the available project data.

The literature shows that structural weight alone does not adequately represent construction complexity. Grouping and rationalization methods primarily simplify structural configurations; penalty-based approaches often employ abstract complexity measures; and detailed cost-estimation methods are rarely incorporated as separate objectives within structural optimization. Moreover, recent developments in automation, BIM, and AI emphasize that complexity costs are measurable but project-dependent. This motivates a unified formulation that separately quantifies different complexities using physically interpretable, dimensionless indices and examines their trade-offs with material consumption within a multi-objective optimization framework.

1.3. Contribution of this work

This study incorporates a parametric criterion of structural complexity intended to capture construction-related effects within structural optimization, as illustrated in Fig. 3. The formulation extends beyond material-based metrics by explicitly accounting for typological diversity, nodal demand, and logistical requirements. These factors reflect fabrication effort, assembly operations, and transportation constraints, which are not directly represented by structural weight alone.

The primary contribution of this work lies in the formulation of three dimensionless and physically interpretable structural complexity indices, namely typological complexity, nodal complexity, and logistical complexity. These indices are defined in normalized, dimensionless form and are directly linked to measurable engineering quantities such as cross-section distribution, member connectivity, and component size. The dimensionless definition expresses each complexity component relative to the material cost and enables consistent comparison among design alternatives evaluated under a common construction scenario. In this way, structural complexity is quantified explicitly rather than treated implicitly through empirical penalties.

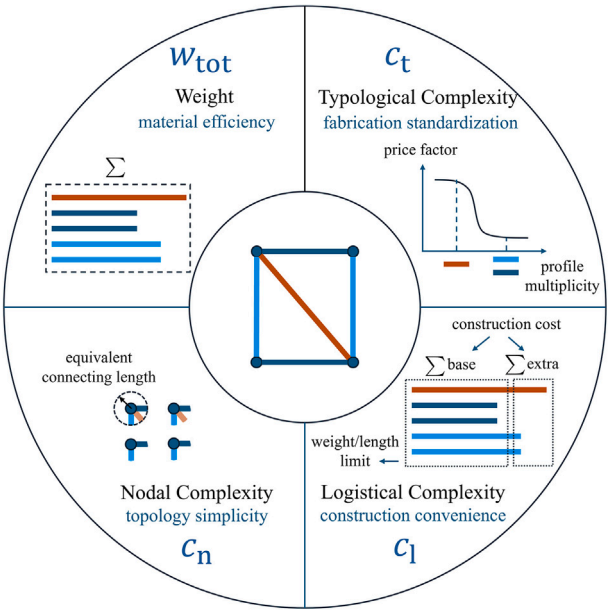

Fig. 3. Concept illustration.

To demonstrate their applicability, the proposed complexity indices are embedded within a standard multi-objective optimization framework together with material weight. This setting enables systematic exploration of trade-offs between material efficiency and construction-related attributes.

By integrating the dimensionless complexity indices into the multi-objective optimization, the framework enables simultaneous assessment and minimization of material consumption and construction-related costs. It provides a quantitative basis for evaluating trade-offs among material efficiency, fabrication standardization, topological simplicity, and logistical convenience, thereby supporting designers' decision-making in early design stages.

1.4. Organization

The rest of the paper is organized as follows: Section 2 introduces the comprehensive cost model. Section 3 illustrates the proposed approach through three case studies: a planar truss cantilever, a three-dimensional geodesic dome, and an industrial steel building. Conclusions are presented in Section 4.

2. Comprehensive cost model

This study focuses on steel structures and aims to establish a comprehensive cost model that explicitly accounts for both material-related and complexity-related cost components. Accordingly, the total cost, denoted as C_{tot}, is decomposed into four parts, given by:

$$C_{tot} = C_{mat} + C_{typ} + C_{nd} + C_{log}. \quad (1)$$

where C_{mat} is the pure material cost, C_{typ} is the fabrication and profile-diversity cost, C_{nd} is the nodal connection cost, and C_{log} is the transport and erection cost.

2.1. Base cost: material consumption

Similar to how it is defined in the classical structural optimization problem, the base material cost C_{mat} is calculated by:

$$C_{\text{mat}} = p_{\text{stl}} \sum_{i=1}^{n_{\text{b}}} w_i = p_{\text{stl}} \rho_{\text{stl}} \sum_{i=1}^{n_{\text{b}}} a_i l_i. \tag{2}$$

where p_{stl} is the unit price of steel, ρ_{stl} is the mass density of the steel, n_{b} is the number of components in the structure, and w_i, a_i, l_i are the weight, cross-sectional area, and length of the i-th member, respectively.

2.2. Typological complexity: fabrication and profile surcharge

Typological complexity is introduced in this study to indirectly account for a portion of the total construction cost associated with profile diversity. The diversity of steel profiles is important in practical engineering (Carvalho et al., 2024), as each distinct profile requires independent procurement, dedicated workshop setup, separate cutting lists, quality control procedures, and specific inventory management. As a result, rarely used profiles (i.e., those adopted only once or twice) are usually associated with higher unit costs, whereas widely used profiles benefit from economies of scale (Stigler, 1958) and standardized production (Azad et al., 2021). Therefore, in the proposed cost model, the unit fabrication cost of each element is assumed to depend on the number of elements sharing the same cross-sectional profile.

The underlying assumptions are as follows: (1) high initial unit costs are incurred for low repetition levels due to setup, specialization, and limited production efficiency; (2) increasing cost benefits are achieved as the degree of standardization and production volume increase; and (3) a lower bound of unit cost reduction is reached when the repetition level becomes sufficiently large. These characteristics are typical of learning-curve and mass-production effects in industrial manufacturing.

Let γ_i denote the typological-cost ratio relative to the base steel price. The typological cost can then be expressed as:

$$C_{\text{typ}} = p_{\text{stl}} \sum_{i=1}^{n_{\text{b}}} \gamma_i w_i. \tag{3}$$

Here γ_i is is modeled using a logistic/sigmoid model, which has also been adopted in the previous study (Lai et al., 2025) as a function to penalize small cross-sectional areas. The curve is shown in Fig. 4. γ_i is determined by the multiplicity number n_i of elements using the same profile, stated as:

$$\gamma_i(n_i) = \gamma_{\min} + \frac{\gamma_{\max} - \gamma_{\min}}{1 + \exp(k(n_i - n^*))}. \tag{4}$$

where $\gamma_{\max}$ is the highest cost factor for rare profiles, and $\gamma_{\min}$ is the minimal cost factor for widely used profiles. k is the learning factor, a rate parameter controlling the steepness of the logistic decrease. n^* is the characteristic repetition level corresponding to the midpoint (inflection point) of the transition, at which the second derivative is equal to zero. n^* can be calculated by a given repetition limit $n_{\lim}$ as $n^* = \frac{1+n_{\lim}}{2}$. The function mathematically satisfies $\lim_{n_i \to -\infty} \gamma_i(n_i) = \gamma_{\max}$, $\lim_{n_i \to +\infty} \gamma_i(n_i) = \gamma_{\min}$, $\gamma_i(n^*) = \frac{\gamma_{\min}+\gamma_{\max}}{2}$, and $\gamma_i''(n^*) = 0$.

2.3. Nodal complexity: equivalent connection demand

The cost of nodes plays a critical role in the total structural cost, and thus has received significant attention in existing studies (Ranalli et al., 2018; Van Mellaert et al., 2016). In practical engineering, node cost is primarily governed by the equivalent amount of connection-related steel, including bolts, welds, gusset plates, and local stiffening components (Havelia, 2016; Jármai & Farkas, 1999; Pavlovčič et al., 2004), as well as the local congestion level and construction accessibility at the nodes.

For the purpose of preliminary structural optimization, this cost is approximated using a simplified model that assumes: (1) the volume of a node is the sum of the connection volumes contributed by all members connected to it, representing the material consumption associated with bolts or welds; (2) each member's connection volume is assumed to be proportional to its cross-sectional size, implying that members with larger cross-sections require proportionally more connecting bolts or weld material. The corresponding proportional factor has the dimension of length and is therefore called the equivalent connection length.

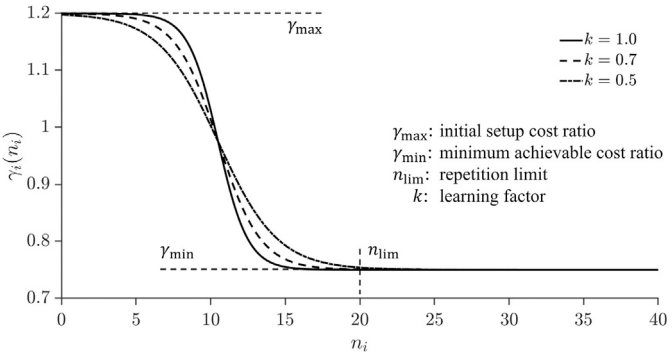

Fig. 4. Logistic/Sigmoid function.

Based on these assumptions, the cost of the nodes C_{nd} can be stated as:

$$C_{\text{nd}} = p_{\text{nd}} \rho_{\text{nd}} \sum_{i=1}^{n_{\text{n}}} v_{\text{n},i} = p_{\text{nd}} \rho_{\text{nd}} \sum_{i=1}^{n_{\text{n}}} \sum_{j=1}^{n_{\text{b},i}} a_{j,i} l_{\text{c},j,i}. \tag{5}$$

where p_{nd} is the unit price of the connection material, ρ_{nd} is its mass density, n_{n} is the number of nodes in the structure, $v_{\text{n},i}$ is the equivalent volume of the i-th node, $n_{\text{b},i}$ is the number of the elements meeting at the i-th node, $a_{j,i}$ is the cross-sectional area of the j-th member connected to the i-th node, and $l_{\text{c},j,i}$ is its equivalent connection length.

Suppose the node material is identical to the connected members (i.e., structural steel), and the equivalent connection length is a constant l_{c} for all members. Then we obtain:

$$C_{\text{nd}} = p_{\text{stl}} \rho_{\text{stl}} \sum_{i=1}^{n_{\text{n}}} \sum_{j=1}^{n_{\text{b},i}} a_{j,i} l_{\text{c}} = p_{\text{stl}} \sum_{i=1}^{n_{\text{n}}} \sum_{j=1}^{n_{\text{b},i}} w_{j,i} \frac{l_{\text{c}}}{l_{j,i}}. \tag{6}$$

where $w_{j,i}$ is the weight of the j-th member connected to the i-th node, and $l_{j,i}$ is its length. Fig. 5 illustrates how the node cost is approximated. l_{c} can be estimated from the connection-material volume associated with bolts, weld metal, etc., per unit member cross-sectional area. Note that if the material of the connection and the member are not identical, l_{c} should be adjusted according to the price and density difference. Meanwhile, l_{c} can also incorporate the effects of construction difficulty, such as welding time and bolt installation effort, through an empirical amplification factor.

For a truss structure where each member connects exactly two nodes and the cross-section is uniform along its length, the double sum in Eq. (6) can be simplified to a sum over members:

$$C_{\text{nd}} = p_{\text{stl}} \sum_{i=1}^{n_{\text{b}}} 2\, w_i \frac{l_{\text{c}}}{l_i}. \tag{7}$$

This expression explicitly shows that each member contributes at both end nodes, thus increasing the number of members tends to increase the nodal cost. Hence, minimizing node cost encourages fewer members, promoting topological simplicity.

2.4. Logistical complexity: transportation and erection

The assembly of fabricated structural components on the construction site is an important component of the total structural cost

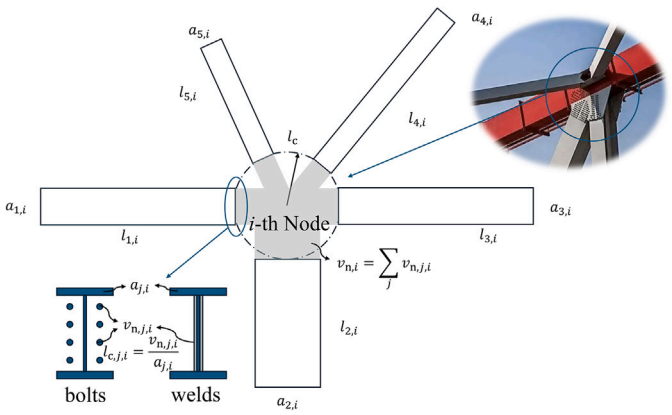

Fig. 5. Equivalent node volume.

(Sarma & Adeli, 2000). The length and weight of each structural element determine the selection of transportation vehicles, lifting cranes, hoisting techniques, and the associated assembly risks. The logistical cost is therefore related not only to the total structural weight but also to the distribution of member lengths and weights, particularly exceedances of standard transportation and lifting thresholds. Elements with moderate lengths and weights are easier to transport and assemble. In contrast, excessively long or heavy members usually require special transportation arrangements and lifting methods, resulting in additional construction costs.

The proposed logistical cost model is established under the following assumptions: (1) the cost of transportation and on-site assembly is assumed to be positively correlated with the total structural weight, reflecting the direct relationship between mass and logistical effort; (2) oversized or overweight members that exceed standard transport or lifting limits require special handling methods, such as dedicated vehicles or cranes, resulting in additional costs.

Accordingly, the cost $C_{\log}$ is stated as:

$$C_{\log} = p_{\log} \sum_{i=1}^{n_b} (1 + \beta_l \delta_{l,i} + \beta_w \delta_{w,i}) w_i. \tag{8}$$

where $p_{\log}$ is the construction price per kg of normal members. β_l and β_w are the oversized and overweight factors for specially long and heavy members. $\delta_{l,i}$ and $\delta_{w,i}$ represent the normalized length and weight exceedances of the i-th member, which can be calculated by:

$$\begin{aligned} \delta_{l,i} &= \max\left(0, \frac{l_i}{l_{\text{ref}}} - 1\right) \\ \delta_{w,i} &= \max\left(0, \frac{w_i}{w_{\text{ref}}} - 1\right). \end{aligned} \tag{9}$$

where l_{ref} and w_{ref} are the reference length and weight thresholds for standard transportation and erection, which can be selected according to national transportation regulations or standard heavy-duty truck specifications.

2.5. Comprehensive cost and dimensionless complexity indices

In the context of this study, structural complexity is interpreted from a construction-oriented perspective. A structure is considered complex if it involves (i) a high diversity of cross-sectional types, leading to reduced standardization; (ii) a large number of members and connections, or intricate topological configurations, increasing assembly effort; and (iii) components that are difficult to transport or lift, such as excessively long or heavy members.

Substituting Eqs. (2), (3), (7), and (8) into Eq. (1) gives:

$$C_{\text{tot}} = p_{\text{stl}} \sum_{i=1}^{n_b} w_i + p_{\text{stl}} \sum_{i=1}^{n_b} \gamma_i w_i + p_{\text{stl}} \sum_{i=1}^{n_b} 2\, w_i \frac{l_c}{l_i} + p_{\log} \sum_{i=1}^{n_b} (1 + \beta_l \delta_{l,i} + \beta_w \delta_{w,i}) w_i. \tag{10}$$

Let $w_{\text{tot}} = \sum_{i=1}^{n_b} w_i$ be the total weight of the structure, and $r_i = \frac{w_i}{w_{\text{tot}}}$ be the relative weight of the i-th member to the structure, then the comprehensive cost can be rewritten as:

$$C_{\text{tot}} = p_{\text{stl}} w_{\text{tot}} \left(1 + \underbrace{\sum_{i=1}^{n_b} \gamma_i r_i}_{c_t} + \underbrace{\sum_{i=1}^{n_b} 2\, r_i \frac{l_c}{l_i}}_{c_n} + \underbrace{\frac{p_{\log}}{p_{\text{stl}}} \sum_{i=1}^{n_b} (1 + \beta_l \delta_{l,i} + \beta_w \delta_{w,i}) r_i}_{c_l} \right). \tag{11}$$

where c_t, c_n, and c_l are the dimensionless complexity indices related to types, nodes and logistics, respectively. They represent the relative contribution of each complexity component to the total cost, expressed as a proportion of the pure material cost.

Let $c = c_t + c_n + c_l$ represent the overall complexity of the structure. The comprehensive cost can be expressed in a simple penalized format as follows:

$$C_{\text{tot}} = p_{\text{stl}} w_{\text{tot}} (1 + c). \tag{12}$$

It is important to note that these complexity components are not independent of structural weight, nor of each other. Reducing material weight often requires increased structural refinement, such as a larger number of members or greater cross-sectional diversity. Conversely, simplifying fabrication, assembly, or logistical costs typically promotes standardization and modularization, which can lead to heavier structural solutions. As a result, inherent conflicts arise between material efficiency and different aspects of construction-related complexity.

2.6. Multi-objective optimization workflow

To capture the trade-off between structural weight and complexity, a multi-objective optimization framework is established following the workflow shown in Fig. 6. The process begins with a preliminary analysis that considers market conditions, fabrication capability, labour cost, site constraints, transport limits, and code regulations. Based on this analysis, key parameters are assigned, including material type and price, section catalog, and complexity-related parameters. The design variables, covering topology, geometry, and sizing, are then defined based on the design flexibility available at the current stage. The objective functions are formulated using the assigned parameters, while structural verifications (strength, stiffness, stability) are imposed as constraints. Then, the total weight w_{tot}, the typological complexity c_t, the nodal complexity c_n, and the logistical complexity c_l are simultaneously minimized:

$$\min_{\boldsymbol{x}} (w_{\text{tot}}, c_t, c_n, c_l) \tag{13}$$

The Genetic Algorithm (GA) is a well-established optimization method capable of handling mixed discrete and continuous variables, multiple local minima, and highly non-linear, non-convex objectives (Holland, 1992; Rajeev & Krishnamoorthy, 1992). It has been demonstrated that GA can optimize steel structures with respect to topology, geometry, and sizing (Kociecki & Adeli, 2015; Zawidzki & Jankowski, 2019). In this study, a multi-objective Non-dominated Sorting Genetic Algorithm II (NSGA-II) (Deb et al., 2002) is employed to investigate the trade-offs among conflicting objectives.

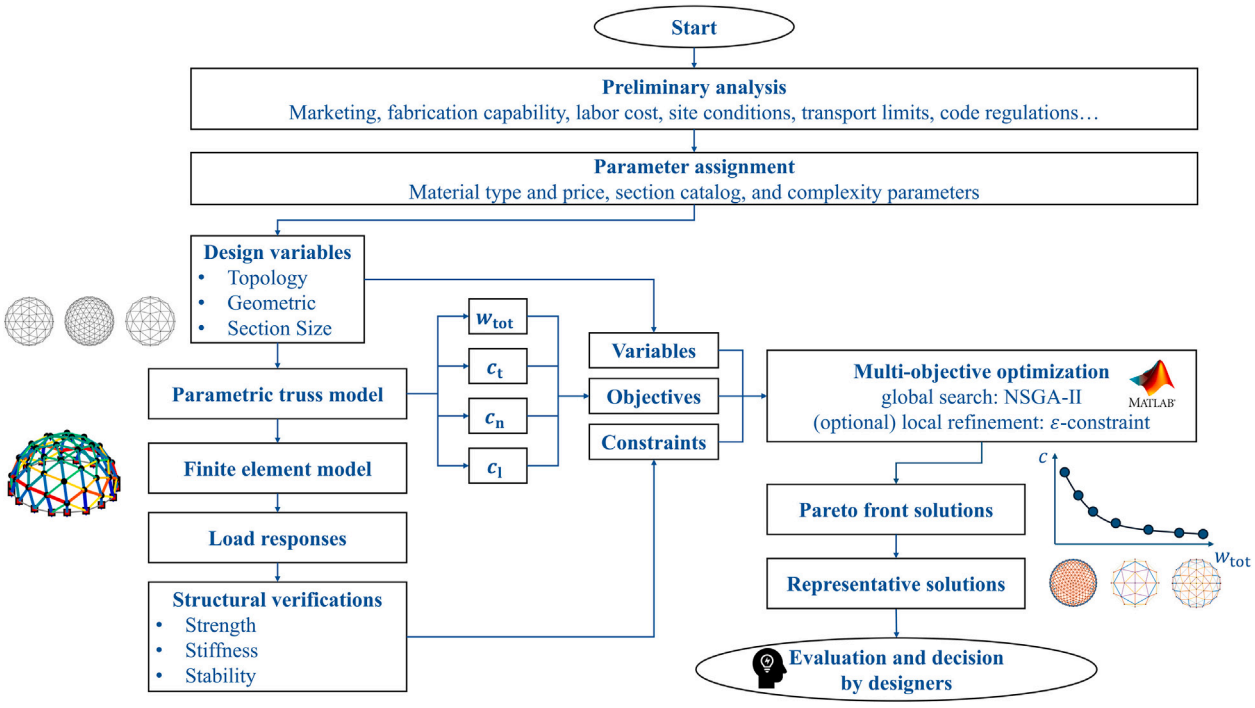

Fig. 6. Workflow.

Table 1
Physical interpretation and required information for identifying the complexity parameters.

Index	Parameter	Meaning	Unit	Required information
–	p_{stl}	Unit material price of structural steel	currency/kg	Steel supplier quotations or procurement records
c_t	γ_{max}	Fabrication-cost ratio for rarely used profiles	–	Normal fabrication cost and rare-profile surcharge per unit mass
c_t	γ_{min}	Standard fabrication-cost ratio for highly repeated profiles	–	Normal fabrication labour or cost per unit mass
c_t	n_{lim}	Repetition level beyond which additional savings are limited	–	Profile repetition and corresponding fabrication labour or cost
c_t	k	Rate of unit-cost reduction with increasing repetition	–	Fabrication labour or cost at different repetition levels
c_n	l_c	Connection cost expressed as an equivalent member length	m	Connection materials and connection-specific fabrication and erection costs
c_l	p_{log}	Baseline transport and erection cost per unit steel mass	currency/kg	Normal transport, lifting, handling, and erection costs
c_l	l_{ref}	Length threshold for standard transport and erection	m	Vehicle, route, fabrication, lifting, and site length limits
c_l	w_{ref}	Weight threshold for standard transport and erection	kg	Vehicle payload, crane capacity, and site handling limits
c_l	β_l	Additional cost factor for members exceeding l_{ref}	–	Additional transport and erection costs for long members
c_l	β_w	Additional cost factor for members exceeding w_{ref}	–	Additional transport and erection costs for heavy members

To improve the local accuracy of the Pareto front obtained by NSGA-II, ε-constraint (EC) method (Haimes, 1971; Mavrotas, 2009) can subsequently be employed to refine the continuous cross-section variables. In each EC subproblem, one objective is minimized while the other is imposed as an inequality constraint with a prescribed upper bound. The resulting scalar problems are solved using a gradient-based Sequential Quadratic Programming (SQP) algorithm (Nocedal & Wright, 1999) with analytical derivatives. The original definitions of c_t and c_l are non-differentiable because they involve a discrete multiplicity count and max operators. To enable gradient-based local refinement, differentiable approximations are introduced in Appendix B, and the corresponding analytical gradients are derived in Appendix C. Nevertheless, NSGA-II remains the appropriate optimization method where the cross-sectional design variables are fully discrete and gradient-based local refinement is not directly applicable.

The Pareto front of the problem provides a set of non-dominated solutions that represent optimal trade-offs among material usage and construction complexity. Finally, designers can select a compromise solution from the Pareto set based on additional considerations, including safety requirements, constructability constraints, and project-specific cost priorities.

2.7. Parameter identification and applicability

The parameters of the proposed cost model are scenario-dependent inputs. The information required to identify each parameter is summarized in Table 1.

The steel price p_{stl} can be obtained directly from supplier quotations or procurement records.

The lower limit γ_{min} corresponds to the normal fabrication cost of standardized profiles produced with sufficient repetition. This cost includes routine operations such as material handling, machine setup, cutting, surface treatment, and inspection (Pavlovčič et al., 2004). The upper limit γ_{max} represents the fabrication cost of rarely used profiles, including the additional effort associated with separate procurement, dedicated setup, cutting lists, production changeovers, and quality control. The parameters can be identified from fabrication labour hours or costs per unit mass recorded at different profile-repetition levels. The normal fabrication rate determines γ_{min}, while the additional effort for small production batches determines γ_{max}. The variation of these records with repetition is then used to determine n_{lim} and k.

The equivalent connection length l_c represents the material and work associated with each member end as an equivalent length of

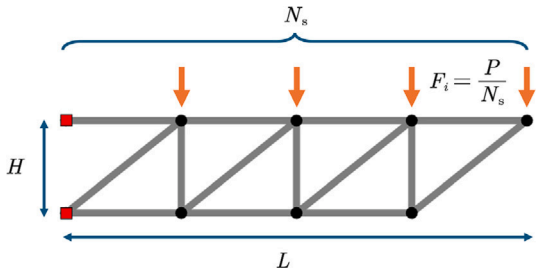

Fig. 7. Case 1: a planar cantilever. $P = 40$ kN.

Table 2
Design variables of case 1.

Design Variables $\boldsymbol{x}$	Type	Symbol	Format	Bounds
number of subdivisions	topology	N_s	discrete integer	5–9
height-span ratio	shape	$\frac{H}{L}$	continuous float	0.15–0.30
cross-sectional area (cluster = 4)*	size	A_1–A_8	continuous float	1–80 cm^2

* the detailed clustering strategy is presented in Appendix A.

structural steel. It can be estimated from representative joints by accounting for plates, bolts, weld consumables, cutting, drilling, fitting, shop welding, and field installation. The resulting connection cost is then converted into an equivalent steel quantity using p_{stl}. A single value represents an average connection assumption at the conceptual design stage, while separate values should be appropriately calibrated for alternative solutions involving substantially different connection systems.

The logistical parameters describe the baseline transport and erection scenario. The price p_{log} can be obtained from contractor quotations or historical records of freight, lifting, handling, equipment, and erection labour. The reference values l_{ref} and w_{ref} represent the largest members handled without special measures and may be selected from vehicle, route, fabrication, crane, and site limits. The factors β_{l} and β_{w} may then be estimated from the additional costs of special transport, permits, larger cranes, or modified erection procedures.

3. Case studies

Three steel structures are tested in this section to demonstrate the effect of the proposed cost model. The material is structural steel S235, with a Young's modulus of $E = 2.1 \times 10^{11}$ Pa and a density of $\rho = 7850$ kg/m^3. The baseline complexity parameters are $\gamma_{\max} = 2$, $\gamma_{\min} = 1$, $k = 0.5$, $n_{\text{lim}} = 200$, $\beta_{\text{l}} = \beta_{\text{w}} = 1$, $l_{\text{c}} = 1$ m, $l_{\text{ref}} = 5$ m, $w_{\text{ref}} = 100$ kg, $p_{\text{log}}/p_{\text{stl}} = 0.5$.

For each case, we used the `ga` function in MATLAB to obtain the single-objective optima and the `gamultiobj` function in MATLAB to obtain the Pareto front. The single-objective GA was repeated 5 times with different random seeds and the best results served as the initial population in the subsequent multi-objective NSGA optimization. The population size was set to 80 for the single-objective case and to 300 for the multi-objective case, with a maximum of 500 generations. All other hyperparameters were kept at their default values in MATLAB.

3.1. Case 1: a planar cantilever truss

Consider ten cantilever trusses arranged in parallel with a span of $L = 30$ m, as illustrated in Fig. 7. For each truss, the structure is fixed at its left boundary and subjected to vertically applied nodal loads, which are distributed over the nodes located along the top edge. The design variables are listed in Table 2. Since the cross-sectional area variables are continuous, the Pareto solutions obtained by NSGA-II can be further refined using the EC method while keeping the discrete topology and geometry variables fixed.

The corresponding constraint functions (with $g \le 0$ defining feasibility) are defined as follows:

$$\begin{cases} g_{1,i} = \frac{N_i}{A_i f_{\text{y}}} - 1, \forall i \in \{1, 2, \dots, n_{\text{b}}\} \\ g_{2,i} = -\frac{N_i}{A_i f_{\text{y}}} - 1, \forall i \in \{1, 2, \dots, n_{\text{b}}\} \\ g_3 = \frac{w_{\text{tot}}}{3 w_{\text{tot,ref}}} - 1 \end{cases} \tag{14}$$

where N_i is the axial force in member i (positive in tension), A_i is the cross-sectional area, and f_{y} is the yield strength of steel. g_3 is set to prevent material overuse in reported solutions and $w_{\text{tot,ref}} = 10^4$ kg.

Fig. 8 presents the trade-offs between the normalized structural weight and the three individual complexity components, together with the overall complexity. All four objective pairs exhibit a clear trade-off between material efficiency and construction-related complexity: reducing structural weight generally increases complexity, while lower-complexity solutions require additional material. The w_{tot}–c_{n} front is smooth and monotonic, whereas the w_{tot}–c_{t} and w_{tot}–c_{l} fronts contain distinct branches caused by changes in section repetition and the activation of member-length or member-weight penalties. These discontinuities are also reflected in the overall w_{tot}–c front, showing that designs with similar weights may have substantially different construction complexities. The combined non-dominated set therefore provides a more complete representation of the achievable trade-offs.

A sensitivity analysis is then performed to examine the influence of the parameters selected through engineering judgment. The results are shown in Fig. 9. Three bi-objective formulations were considered separately: w_{tot}–c_{t}, w_{tot}–c_{n}, and w_{tot}–c_{l}. For the typological index, the investigated levels were $\gamma_{\max} = \{1.5, 2.0, 2.5\}$, $\gamma_{\min} = \{0.5, 1.0, 1.5\}$, $k = \{0.25, 0.50, 0.75\}$, and $n_{\text{lim}} = \{100, 200, 300\}$. The nodal parameter was varied as $l_{\text{c}} = \{0.5, 1.0, 1.5\}$ m. For the logistical index, β_{l} and β_{w} were varied jointly as $\{0.5, 1.0, 1.5\}$, while the reference limits were varied jointly as $(l_{\text{ref}}, w_{\text{ref}}) = \{(2.5\,\text{m}, 50\,\text{kg}), (5\,\text{m}, 100\,\text{kg}), (7.5\,\text{m}, 150\,\text{kg})\}$.

It shows that the general trade-off between structural weight and construction complexity is retained under the investigated parameter variations, although the position and spread of the Pareto fronts change. The typological results are most sensitive to n_{lim}, followed by $\gamma_{\max}$ and $\gamma_{\min}$, whereas variations in k produce comparatively limited changes. Changing l_{c} primarily rescales the nodal-complexity objective and does not change the ordering of the candidate designs. For logistical complexity, the joint variation of β_{l} and β_{w} causes moderate changes, while the reference limits l_{ref} and w_{ref} have a stronger influence because they determine which members are treated as exceeding the baseline transport and erection capacity.

3.2. Case 2: a three-dimensional geodesic dome

The dome has a radius of $R = 20$ m, as illustrated in Fig. 10. The truncation ratio is 0.5. A non-structural roof covering load $q = 0.5$ kN/m^2 is applied along with structural self-weight ($g = 9.8$ m/s^2). Partial safety factor $\gamma_{\text{G}} = 1.35$ is applied to both dead-load components. The distributed q is transformed into uniform concentrated vertical nodal loads at the nodes. The design variables are listed in Table 3.

The corresponding constraint functions are defined as follows:

$$\begin{cases} g_{1,i} = \frac{N_i}{A_i f_{\text{y}}} - 1, \forall i \in \{1, 2, \dots, n_{\text{b}}\}, \text{ ULS} \\ g_{2,i} = -\frac{N_i}{A_i f_{\text{y}}} - 1, \forall i \in \{1, 2, \dots, n_{\text{b}}\}, \text{ ULS} \\ g_{3,i} = -\frac{N_i}{\chi_i A_i f_{\text{y}}} - 1, \forall i \in \{1, 2, \dots, n_{\text{b}}\}, \text{ ULS} \\ g_4 = \frac{w_{\text{tot}}}{5 w_{\text{tot,ref}}} - 1 \end{cases} \tag{15}$$

where N_i is the axial force in member i (positive in tension), A_i is the cross-sectional area, and f_{y} is the yield strength of steel. The reduction factor χ_i accounts for member buckling according to Eurocode 3 and is determined as a function of the non-dimensional slenderness. g_4 is set to prevent material overuse in reported solutions and $w_{\text{tot,ref}} = 10^4$ kg.

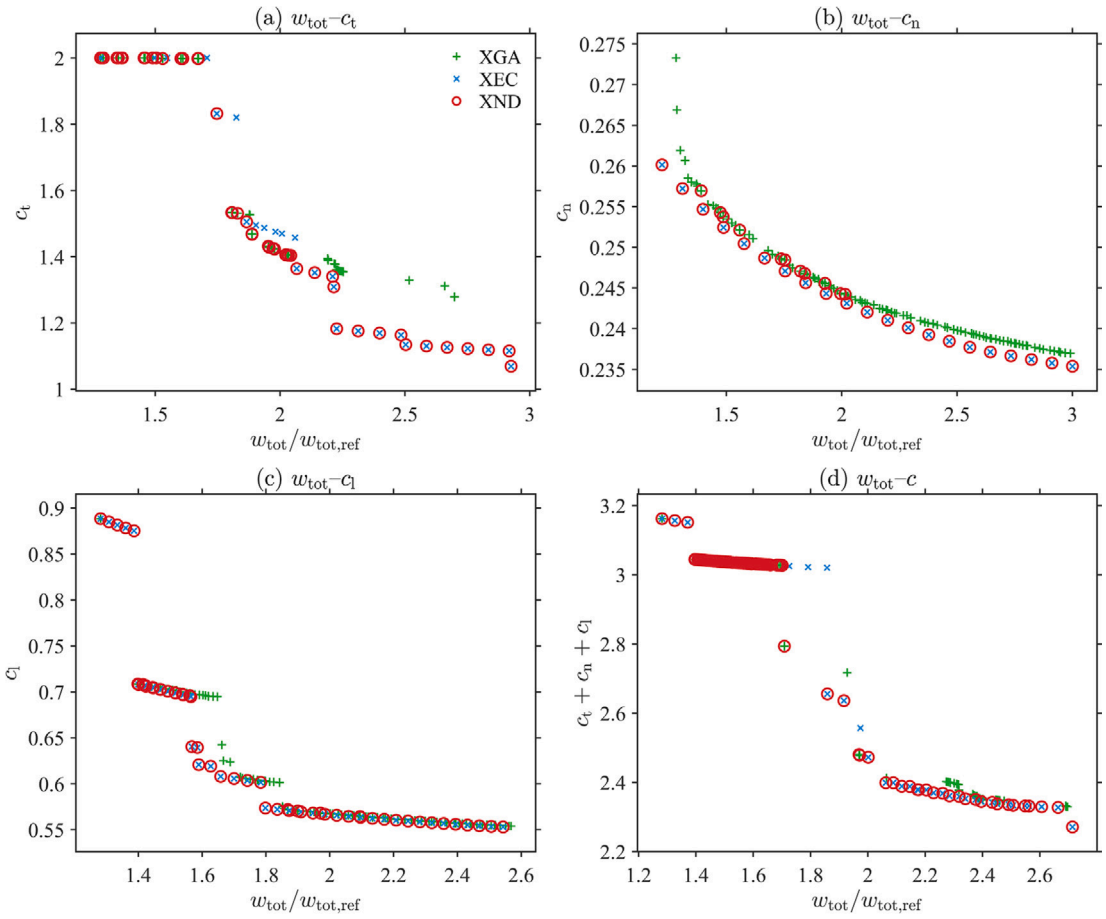

Fig. 8. Bi-objective Pareto fronts for Case 1. XGA and XEC denote the feasible solutions generated by global search (NSGA) and local refinement (EC), respectively, while XND denotes the non-dominated solutions extracted from their union.

Table 4 and Fig. 11 present the results of the single-objective optimization. All results reported in the table are feasible.

The results reveal distinct conflicts among the material and complexity objectives. As shown in Fig. 11(a), minimizing structural weight requires a relatively large variety of cross-section profiles, resulting in high typological complexity. Conversely, the minimum-c_t design in Fig. 11(b) uses fewer section profiles but contains substantially more members and a greater structural weight. The minimum-c_n design in Fig. 11(c) has a much simpler topology, although its members are considerably longer and heavier, thereby increasing transportation and erection demands. In contrast, minimizing logistical complexity produces the highly subdivided design shown in Fig. 11(d), in which the individual members are shorter and lighter but the numbers of members and nodes increase. Finally, Fig. 11(e) presents a compromise between material efficiency and the different complexity components, as obtained by minimizing the comprehensive cost defined in Eq. (1).

The Pareto front is further examined for Case 2. A total of 105 non-dominated solutions were obtained by simultaneously minimizing the normalized structural weight, typological complexity, and nodal complexity. The resulting three-dimensional Pareto front is shown in Fig. 12.

The Pareto solutions cover a wide range of structural weights, $0.799 \leq w_{tot}/w_{tot,ref} \leq 4.357$, demonstrating substantial conflicts among the three objectives. The minimum-weight solution has $w_{tot}/w_{tot,ref} = 0.799$, but its typological complexity approaches the upper limit ($c_t = 1.997$). Conversely, the minimum-c_t solution achieves $c_t = 1.000$ through extensive section standardization, while its normalized weight increases to 4.309 and its nodal complexity increases to $c_n = 0.666$. The minimum-c_n solution exhibits a simpler structural topology, with $c_n = 0.160$ and $w_{tot}/w_{tot,ref} = 1.346$, but retains a high typological complexity of $c_t = 2.000$.

The results show that in this case structural weight is negatively correlated with typological complexity but positively correlated with nodal complexity. The front also contains several distinct branches, reflecting transitions between discrete topological configurations and section assignments. Although logistical complexity is not included as an objective axis in this analysis, the minimum-c_t region also approaches the minimum logistical complexity, whereas the minimum-c_n solution contains substantially longer and heavier members. These trends are consistent with the single-objective results presented in Table 4.

Table 5 further compares the proposed formulation with two literature-based cost objectives under the same design space and structural constraints. The reference formulations produce lightweight solutions, only 2.3% and 3.2% heavier than the minimum-weight design, while using 4 and 3 section profiles, respectively. However, this simplification is achieved through substantially longer and heavier members: the maximum member length reaches 13.43 m and the maximum member weight reaches 269.91 kg, compared with 6.50 m and 50.49 kg for the proposed solutions. This demonstrates that reducing member or profile-related fabrication complexity may transfer complexity

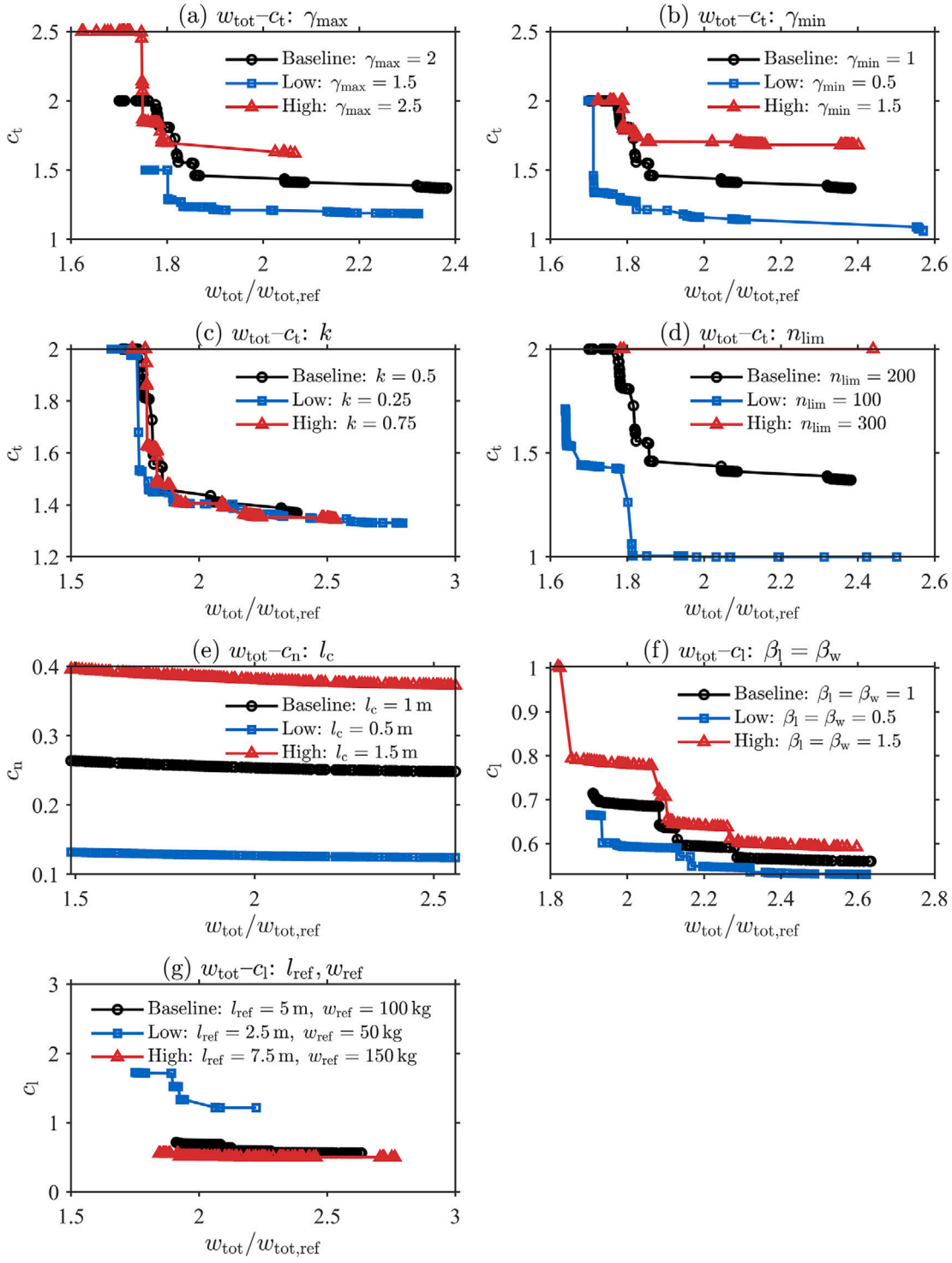

Fig. 9. Sensitivity of the Pareto fronts for Case 1: effects of (a) γ_{max}, (b) γ_{min}, (c) k, and (d) n_{lim} on the w_{tot}–c_t problem; (e) l_c on the w_{tot}–c_n problem; (f) the joint variation of β_l and β_w; and (g) the joint variation of l_{ref} and w_{ref} on the w_{tot}–c_l problem.

to transportation and erection. The comprehensive-cost formulation increases structural weight by 12.2%, but achieves greater section repetition while retaining considerably smaller individual members. The multi-objective optimization framework Eq. (13) can also provide other intermediate alternatives such as the MO low-weight compromise in Table 5.

3.3. Case 3: an industrial steel building

The building under investigation is located in the Mirafiori industrial district, southwest of Turin, Italy. It occupies a site that was formerly part of the well-known FIAT company's operations, with construction dating back to the early 1960s.

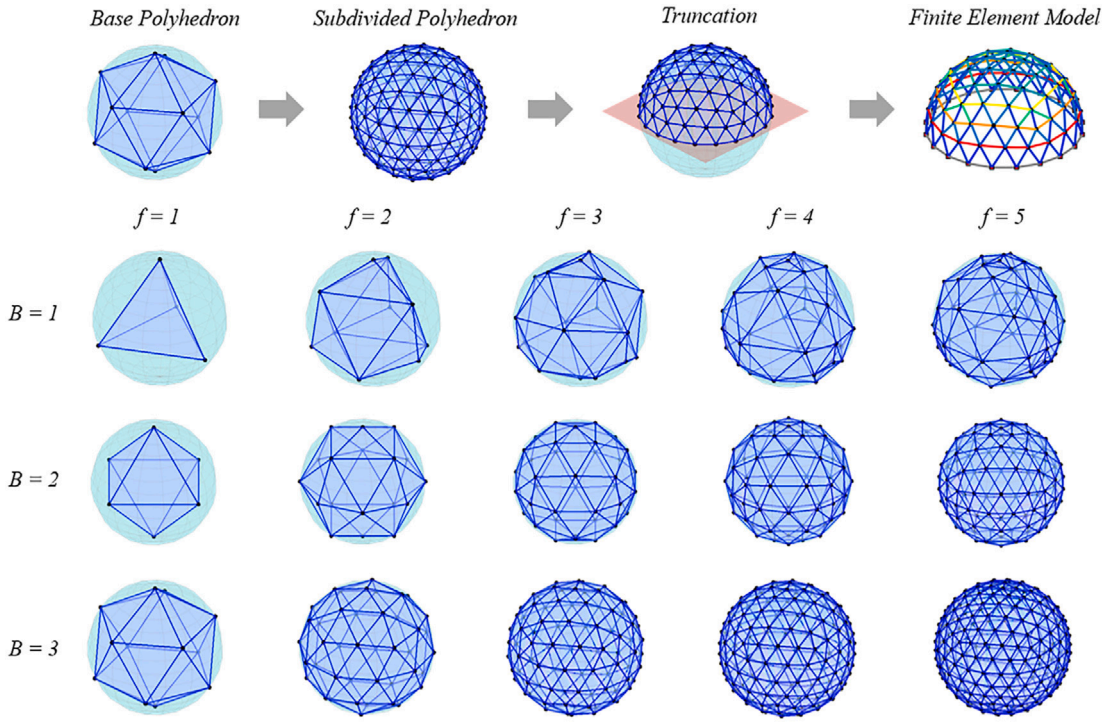

Fig. 10. Case 2: a three-dimensional geodesic dome.

Table 3
Design variables of case 2.

Design Variables $\boldsymbol{x}$	Type	Symbol	Format	Bounds
base polyhedron	topology	B	integer	1–3
frequency	topology	f	integer	3–8
cross section indexes* (cluster = 5)	size	A_1–A_{10}	integer	1–50

* circular hollow steel (CHS) section profiles defined in Eurocode 3, Sections 6.2 and 6.3.

The structure has a span of $L_y = 20$ m and $L_x = 60$ m, and a height of $H = 5$ m, as illustrated in Fig. 13. The structural system consists of roof trusses spanning in the y-direction, supported by columns. Purlins are arranged along the longitudinal x-direction to support the roof cladding, while longitudinal and roof bracings are provided to ensure global stability. The structure is analyzed using a parametric modeling approach in this case.

The design variables and the loads are listed in Tables 6 and 7, respectively.

The adopted load combinations for the ultimate limit state (ULS) and serviceability limit state (SLS) are expressed as:

$$\begin{aligned} &\text{ULS:} \quad \gamma_G G + \gamma_{Q,1} Q_{k,1} + \gamma_{Q,2}\psi_{0,2} Q_{k,2} + \dots \\ &\text{SLS:} \quad G + Q_{k,1} + \psi_{0,2} Q_{k,2} + \dots \end{aligned} \tag{16}$$

where G denotes the permanent structural and non-structural loads, while $Q_{k,1}$ and $Q_{k,2}$ represent the characteristic variable actions. The coefficients γ are the partial safety factors associated with each type of load, and ψ is the combination factor accounting for the reduced probability of simultaneous occurrence of variable actions. In the present study, the most critical load combination is considered.

The safety constraints are formulated in accordance with Eurocode 3 (European Committee for Standardization, 2005). Columns and purlins, modelled as beam members, are verified for cross-section resistance under combined axial force and biaxial bending as well as for member stability at the ultimate limit state (ULS). Bracing and truss members, modelled as axially loaded bar elements, are assumed to carry axial force only; therefore, only axial resistance and buckling checks are considered. In addition, serviceability limit state (SLS) requirements are imposed by limiting the nodal displacements. The corresponding

Table 4
Comparison of optimization results under different single objectives in Case 2.

Objective	Run	w_{tot} (10^4 kg)	c_t	c_n	c_l	c	$w_{tot}(1+c)$ (10^4 kg)
min w_{tot}	**1**	**0.799**	**1.997**	**0.334**	**0.601**	**2.933**	**3.140**
	2	0.841	2.000	0.213	1.117	3.330	3.641
	3	0.858	2.000	0.213	1.115	3.328	3.714
	4	0.835	2.000	0.319	0.647	2.967	3.312
	5	0.837	2.000	0.164	1.813	3.977	4.163
min c_t	1	1.394	1.000	0.665	0.500	2.165	4.413
	2	4.915	1.000	0.666	0.500	2.166	15.564
	3	4.199	1.000	0.665	0.500	2.165	13.288
	4	**4.599**	**1.000**	**0.666**	**0.500**	**2.166**	**14.561**
	5	4.633	1.000	0.666	0.500	2.166	14.666
min c_n	1	1.396	2.000	0.160	2.246	4.406	7.549
	2	1.286	2.000	0.160	2.186	4.346	6.876
	3	1.385	2.000	0.160	2.260	4.420	7.508
	4	**1.346**	**2.000**	**0.160**	**2.224**	**4.384**	**7.248**
	5	1.422	2.000	0.160	2.299	4.459	7.764
min c_l	1	3.486	1.261	0.665	0.500	2.426	11.944
	2	**3.074**	**1.185**	**0.667**	**0.500**	**2.352**	**10.305**
	3	2.775	1.279	0.664	0.500	2.443	9.553
	4	4.406	1.159	0.663	0.500	2.323	14.638
	5	3.264	1.201	0.666	0.500	2.367	10.993
min$[w_{tot}(1+c)]$	1	0.922	1.208	0.336	0.599	2.142	2.898
	2	0.955	1.093	0.334	0.601	2.029	2.893
	3	**0.896**	**1.099**	**0.337**	**0.598**	**2.033**	**2.717**
	4	0.871	1.354	0.369	0.573	2.296	2.871
	5	0.915	1.202	0.335	0.600	2.137	2.871

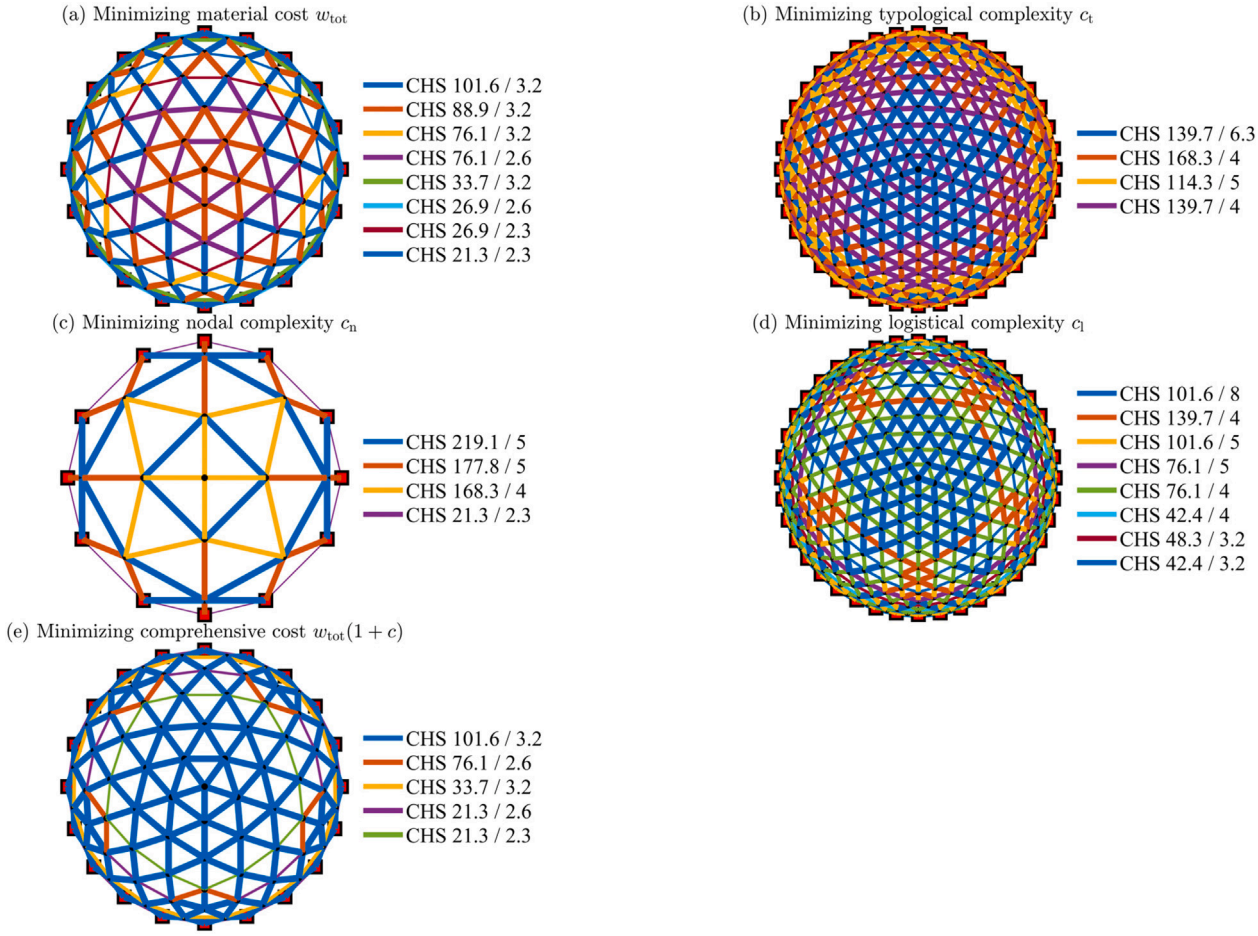

Fig. 11. Optimal dome designs obtained under different single objectives.

constraint functions are defined as follows:

$$\begin{cases} g_{1,i} = \dfrac{N_i}{N_{\mathrm{pl,Rd},i}} + \sqrt{\left(\dfrac{M_{\mathrm{y},i}}{M_{\mathrm{pl,Rd,y},i}}\right)^2 + \left(\dfrac{M_{\mathrm{z},i}}{M_{\mathrm{pl,Rd,z},i}}\right)^2} - 1, \forall i \in \{1,2,\ldots,n_\mathrm{b}\},\ \mathrm{ULS} \\ g_{2,i} = \dfrac{N_i}{\chi_{\mathrm{y},i} N_{\mathrm{pl,Rd},i}} + k_{\mathrm{yy},i}\dfrac{M_{\mathrm{y},i}}{\chi_{\mathrm{LT},i} M_{\mathrm{pl,Rd,y},i}} + k_{\mathrm{yz},i}\dfrac{M_{\mathrm{z},i}}{M_{\mathrm{pl,Rd,z},i}} - 1, \forall i \in \{1,2,\ldots,n_\mathrm{b}\},\ \mathrm{ULS} \\ g_{3,i} = \dfrac{U_i}{L_\mathrm{y}/200} - 1, \forall i \in \{1,2,\ldots,n_\mathrm{n}\},\ \mathrm{SLS} \\ g_4 = \dfrac{w_\mathrm{tot}}{10 w_{\mathrm{tot,ref}}} - 1 \end{cases} \tag{17}$$

where N_i is the axial force, $M_{\mathrm{y},i}$ and $M_{\mathrm{z},i}$ are the bending moments about the principal axes, U_i is the magnitude of the relevant nodal displacement, $N_{\mathrm{pl,Rd},i} = A_i f_\mathrm{y}$, $M_{\mathrm{pl,Rd,y},i} = W_{\mathrm{y},i} f_\mathrm{y}$, and $M_{\mathrm{pl,Rd,z},i} = W_{\mathrm{z},i} f_\mathrm{y}$ are the plastic resistances, $\chi_{\mathrm{y},i}$ and $\chi_{\mathrm{LT},i}$ are the buckling and lateral–torsional reduction factors, $k_{\mathrm{yy},i}$ and $k_{\mathrm{yz},i}$ are the interaction factors according to Eurocode 3, A_i is the cross-sectional area, $W_{\mathrm{y},i}$ and $W_{\mathrm{z},i}$ are the plastic section moduli, f_y is the yield strength, and L_y is the truss span. g_4 is set to prevent material overuse in reported solutions and $w_{\mathrm{tot,ref}} = 10^4$ kg.

The resulting Pareto set is presented using parallel coordinates in Fig. 14. Representative Pareto solutions are shown in Fig. 15. Table 8 presents the features of the representative solutions. The results clearly illustrate how emphasizing different objectives leads to fundamentally different structural configurations.

The minimum-weight solution ($\min w_\mathrm{tot}$) achieves the lowest structural mass (3.36×10^4 kg), thereby minimizing material consumption and associated material cost. This configuration represents the most material-efficient design among all candidates. However, its

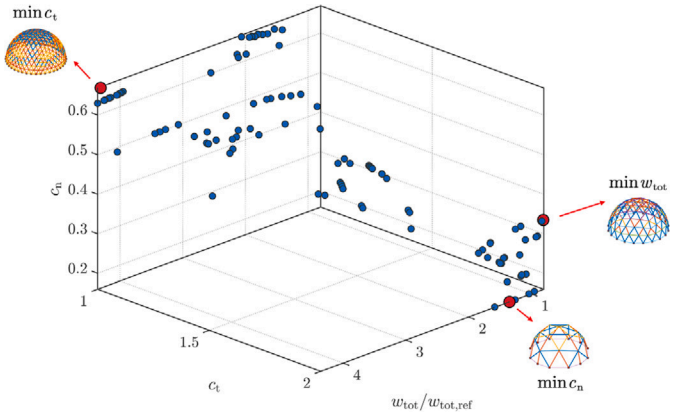

Fig. 12. Three-objective Pareto front for Case 2, including the representative minimum-weight, minimum-typological-complexity, and minimum-nodal-complexity designs.

average profile multiplicity (61) remains moderate, implying limited standardization benefits in fabrication. The relatively large maximum deflection (77.9 mm) also indicates that material savings are obtained at the expense of structural stiffness.

The typological-complexity-oriented solution ($\min c_t$) adopts only four section profiles and achieves an exceptionally high average multiplicity (345). Such intensive reuse of section types maximizes

Table 5
Comparison of the proposed framework with existing cost-based optimization approaches.

Objective function	w_{tot} (kg)	Δw_{tot} (%)	N_p	$\bar{n}_{rep}$	$l_{bar,max}$ (m)	$w_{bar,max}$ (kg)
Minimum weight: $\min w_{tot}$	7985.7	0.0	8	31.2	6.50	50.49
Asadpoure et al. (2015):$\min \frac{w_{tot}+\mu_F N_m}{w_{tot,ref}}$	8168.9	2.3	4	15.0	13.43	269.91
Cucuzza et al. (2024): $\min \frac{w_{tot}}{w_{tot,ref}}\phi_{N_s}\phi_f$	8242.5	3.2	3	20.0	13.43	269.91
Proposed Eq. (11): $\min \frac{w_{tot}(1+c_t+c_n+c_l)}{w_{tot,ref}}$	8958.3	12.2	5	50.0	6.50	50.49
MO low-weight compromise: $\min_{x\in\mathcal{P}_{LW}}(c_t+c_n+c_l)$	8474.5	6.1	7	35.7	6.50	50.49

N_p is the number of distinct section profiles, and $\bar{n}_{rep} = N_m/N_p$ is the average number of members assigned to each profile. $\mathcal{P}_{LW}$ denotes the feasible Pareto subset with no more than a 10% increase in w_{tot} and no more than a 2% increase in either c_n or c_l, relative to the minimum-weight Pareto solution.

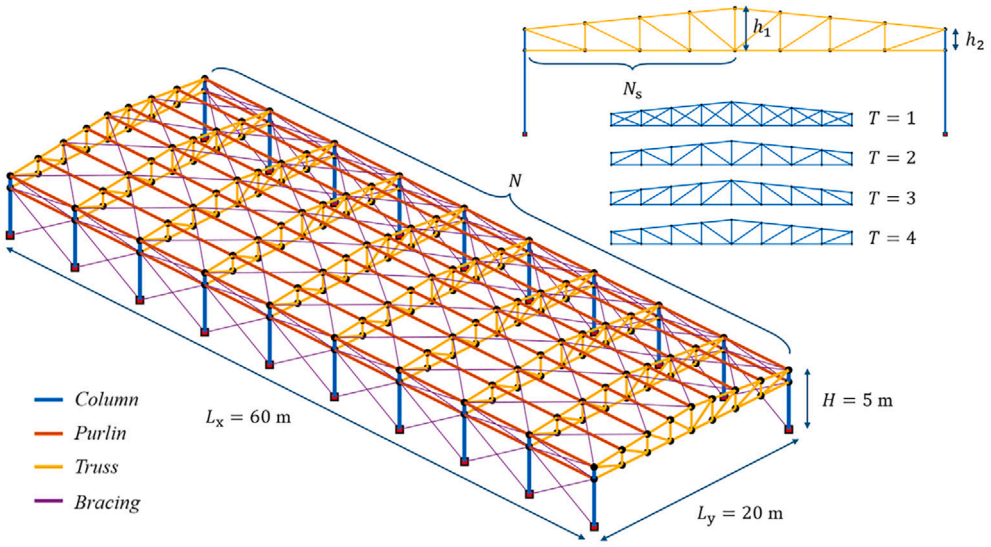

Fig. 13. Case 3: an industrial steel building.

Table 6
Design variables of case 3.

Design Variables x	Type	Symbol	Format	Bounds
truss topology	topology	T	discrete integer	1–4
truss subdivisions (half)	topology	N_s	discrete integer	2–8
truss modules number	topology	N	discrete integer	6–12
truss height-to-span ratio	geometry	$\frac{h_1}{L_y}$	continuous float	0.03–0.1
truss side-to-mid-height ratio	geometry	$\frac{h_2}{h_1}$	continuous float	0.5–1
truss cross section (CHS) indexes (cluster = 3)	sizing	A_1–A_6	discrete integer	1–50
column cross section (HEA) index	sizing	A_7	discrete integer	1–24
purlin cross section (IPE) index	sizing	A_8	discrete integer	1–18
bracing cross section (CHS) index	sizing	A_9	discrete integer	1–25

Table 7
Loads and combinations of case 3.

Load Name	Symbol	Load Value	Partial Factor γ	Combination Factor ψ
structural weight	G_1	$g = 9.8$ m/s^2	1.35	–
non-structural roof weight	G_2	0.05 kN/m^2	1.35	–
maintenance	Q_m	0.4 kN/m^2	1.5	0.7
snow	Q_s	1.23 kN/m^2	1.5	0.5
wind*	Q_w	$q_p = 0.6$ kN/m^2	1.5	0.6

* pressure factor $c = 1, -0.7, -1.1, -0.7$ for the windward wall, leeward wall, windward roof, and leeward roof, respectively.

standardization and enables strong economies of scale in manufacturing, procurement, and quality control. Although the total structural weight increases significantly, the reduction in profile variety lowers production complexity and unit fabrication cost. From an industrialized construction perspective, this solution prioritizes manufacturing efficiency over material minimization.

The nodal-complexity-oriented solution ($\min c_n$) achieves the minimum number of nodes (96), resulting in the simplest structural topology and the smallest number of members. This reduction in joints simplifies fabrication detailing and on-site assembly, and leads to a topologically simpler configuration. However, the simplification of topology is

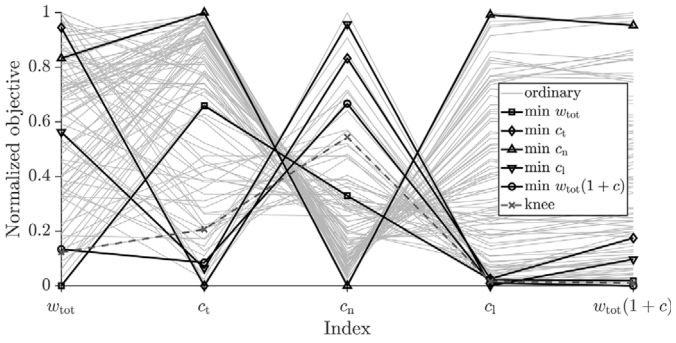

Fig. 14. Parallel coordinates Pareto front.

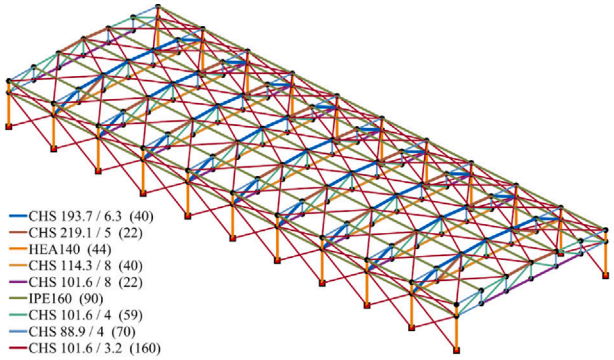

(a) Minimizing material cost w_{tot}.

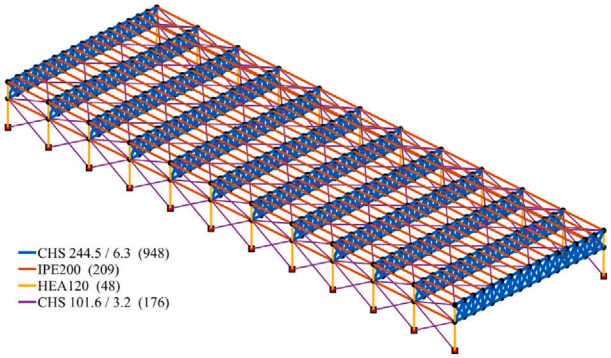

(b) Minimizing typological complexity c_{t}.

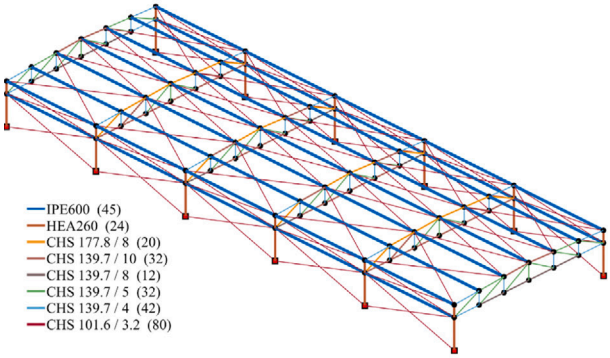

(c) Minimizing nodal complexity c_{n}.

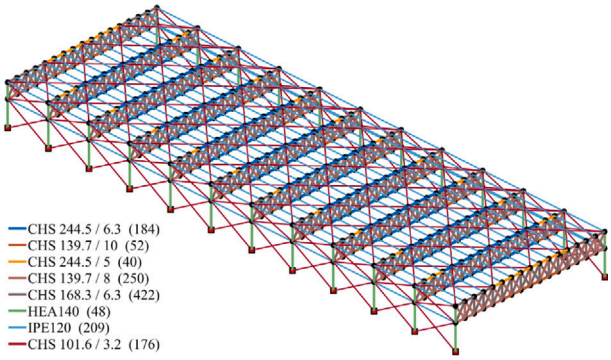

(d) Minimizing logistical complexity c_{l}.

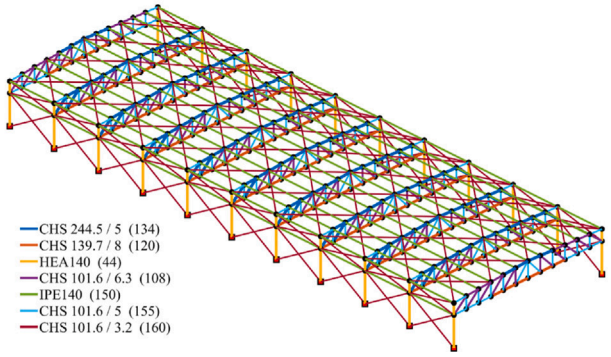

(e) Minimizing comprehensive cost $w_{\text{tot}}(1+c)$.

Fig. 15. Representative Pareto solutions obtained through multi-objective optimization.

Table 8
Quantitative metrics of representative Pareto solutions for Case 3.

Representative solution	w_{tot} (10^4 kg)	N_{p}	$\bar{n}_{\text{rep}}$	N_{n}	$w_{\text{bar,max}}$ (kg)	$l_{\text{bar,max}}$ (m)	U_{max} (mm)
$\min w_{\text{tot}}$	3.36	9	61	176	105.53	8.98	77.9
$\min c_{\text{t}}$	10.00	4	345	432	122.18	7.40	43.3
$\min c_{\text{n}}$	8.81	8	36	96	1468.80	13.73	65.1
$\min c_{\text{l}}$	7.04	8	173	432	78.35	7.40	43.1
$\min [w_{\text{tot}}(1+c)]$	4.24	7	124	308	90.58	7.82	59.6

Note: N_{p} is the number of distinct section profiles, $\bar{n}_{\text{rep}}$ is the average profile multiplicity, N_{n} is the number of nodes, and U_{max} is the maximum nodal displacement.

accompanied by substantially heavier and longer members (maximum bar weight 1468.8 kg; maximum length 13.73 m), which may increase transportation and lifting demands. Thus, while joint complexity is minimized, transportation and lifting demands associated with individual members increase.

The logistical-complexity-oriented solution ($\min c_{\text{l}}$) produces the lightest individual members (maximum bar weight 78.35 kg) and relatively short maximum bar lengths. Such characteristics facilitate transportation, handling, and installation, making this configuration particularly favorable from a construction logistics standpoint. Nevertheless,

Table 9
Cross-case comparison between the minimum-weight and minimum-comprehensive-cost solutions.

Case	$w_{tot}/w_{tot,ref}\|_{\min w_{tot}}$	$w_{tot}/w_{tot,ref}\|_{\min C_{tot}}$	Δw_{tot} (%)	$c\|_{\min w_{tot}}$	$c\|_{\min C_{tot}}$	Δc (%)	I_t (%)	I_n (%)	I_l (%)	Dominant index	MO generations
Case 1	1.282	1.282	0.0	3.162	3.162	0.0	–	–	–	–	178–242
Case 2	0.799	0.896	12.2	2.933	2.033	−30.7	99.4 ↓	0.3 ↑	0.4 ↓	c_t	102
Case 3	3.363	4.237	26.0	2.526	1.769	−30.0	83.6 ↓	11.6 ↑	4.9 ↓	c_t	111

Note: The arrows indicate whether each complexity component decreases (↓) or increases (↑).

Table 10
Changes in construction-related quantitative metrics for representative solutions in the three case studies.

Case	Representative comparison	w_{tot} (10^3 kg)	N_p	$\bar{n}_{rep}$	N_n	$l_{bar,max}$ (m)	$w_{bar,max}$ (kg)
Case 1	$\min w_{tot} \rightarrow \min c$	12.82 → 24.09 (+87.9%)	8 → 4 (−50.0%)	22.5 → 75.0 (+233.3%)	110 → 170 (+54.5%)	9.99 → 7.15 (−28.4%)	150.42 → 154.50 (+2.7%)
Case 2	$\min w_{tot} \rightarrow \min[w_{tot}(1+c)]$	7.986 → 8.958 (+12.2%)	8 → 5 (−37.5%)	31.25 → 50.00 (+60.0%)	91 → 91 (0.0%)	6.50 → 6.50 (0.0%)	50.49 → 50.49 (0.0%)
Case 3	$\min w_{tot} \rightarrow \min[w_{tot}(1+c)]$	33.63 → 42.37 (+26.0%)	9 → 7 (−22.2%)	60.8 → 124.4 (+104.7%)	176 → 308 (+75.0%)	8.98 → 7.82 (−12.9%)	105.53 → 90.58 (−14.2%)

Note: N_p is the number of section profiles, $\bar{n}_{rep}$ is the average profile multiplicity, and N_n is the number of nodes. For Case 1, the solutions minimizing w_{tot} and $w_{tot}(1+c)$ coincide; therefore, the minimum-c solution is used to provide a meaningful comparison.

this benefit is achieved with a high number of nodes (432), implying increased joint fabrication effort.

Finally, the composite objective $\min w_{tot}(1+c)$ yields a compromise solution. The structural weight increases by 26.0% relative to the minimum-weight design, while remaining substantially below that of the extreme complexity-minimizing solutions. Profile multiplicity (124) is substantially improved relative to $\min w_{tot}$, indicating enhanced standardization. Node count and member sizes are also maintained within intermediate ranges. This demonstrates that incorporating complexity-related terms effectively moderates extreme structural tendencies and promotes solutions that balance material efficiency, manufacturing rationality, and constructability.

Overall, each representative solution corresponds to a distinct preference-dominated region: material efficiency ($\min w_{tot}$), manufacturing standardization ($\min c_t$), topological simplicity ($\min c_n$), and logistical convenience ($\min c_l$). This clear separation of optima across different criteria highlights the effectiveness of the proposed dimensionless complexity indices in capturing complementary construction-related attributes beyond material weight. The composite formulation shifts the solution toward a more balanced region of the Pareto set, providing competitive candidates for further project-specific evaluation.

3.4. Summary and cross-case comparison

To provide a consistent cross-case comparison, the minimum-weight solution is compared with the solution minimizing the overall complexity objective c or the comprehensive objective $w_{tot}(1+c)$ for all three cases. The impact share I_j measures the relative contribution of each complexity component to the change between the two representative solutions:

$$I_j = \frac{\left| c_j^{(\min C_{tot})} - c_j^{(\min w_{tot})} \right|}{\sum_{k\in\{t,n,l\}} \left| c_k^{(\min C_{tot})} - c_k^{(\min w_{tot})} \right|} \times 100\%, \qquad j \in \{t,n,l\}. \tag{18}$$

Table 9 shows that the effect of the comprehensive objective depends on the structural system. For the planar truss in Case 1, the minimum-weight solution also minimizes the comprehensive cost, indicating that the attainable complexity reductions are insufficient to justify additional material under the adopted parameters. In Cases 2 and 3, the comprehensive objective increases structural weight by 12.2% and 26.0%, respectively, while reducing overall complexity by 30.7% and 30.0%. Typological complexity is the dominant component in both cases, whereas nodal complexity increases slightly, indicating that improved section standardization may be accompanied by a more subdivided topology. The Case 1 bi-objective searches required 178–242 generations with local refinement. The Pareto searches in Cases 2 and 3 converged after 102 and 111 generations, respectively.

Table 10 demonstrates that the complexity-oriented solutions produce measurable changes in the physical drivers of fabrication, assembly, and logistics. In Case 1, the number of section profiles is reduced from 8 to 4 and the average profile multiplicity increases from 22.5 to 75.0, while the maximum member length decreases by 28.4%. These benefits are accompanied by increases in structural weight and node count. In Case 2, the minimum-comprehensive-cost solution reduces the number of section profiles from 8 to 5 and increases the average multiplicity from 31.25 to 50.00 without increasing the number of nodes or the maximum member length and weight. In Case 3, the number of section profiles decreases from 9 to 7, the average multiplicity approximately doubles, and the maximum member length and weight decrease by 12.9% and 14.2%, respectively, although the structural weight and number of nodes increase. These results provide indirect quantitative evidence of improved fabrication standardization and reduced member-handling demands; however, directly quantifying labour-hour reductions or shorter construction durations would require additional process-specific information and a detailed fabrication and construction scheduling model.

4. Conclusion

Material weight alone does not fully reflect the total construction cost of steel structures, as fabrication, assembly, and transportation requirements introduce additional construction-related implications that are not captured in conventional weight-driven optimization. Addressing this limitation requires structural complexity to be treated as an explicit and quantifiable design attribute.

In this study, three dimensionless and physically interpretable structural complexity indices, namely typological, nodal, and logistical, are formulated to characterize construction-related attributes beyond material consumption. The proposed indices are incorporated alongside material weight within a multi-objective optimization setting, allowing systematic exploration of trade-offs between structural efficiency and constructability-related considerations.

The effectiveness of the proposed complexity indices is evaluated through three representative test cases: a planar cantilever truss, a three-dimensional geodesic dome, and an industrial steel building. In all cases, incorporating complexity measures produces Pareto-optimal solutions that differ from those obtained by weight-only optimization. Consistent trade-offs are observed: lightweight designs tend to exhibit higher typological diversity, whereas reduced construction-related complexity generally requires additional material. The indices show stable and physically interpretable trends across different structural systems,

supporting their role as a complementary design dimension at the conceptual stage.

While the results highlight the potential of incorporating dimensionless complexity measures into structural optimization, the present study remains subject to certain assumptions and scope limitations. It should be noted that the proposed complexity indices are indirect measures intended to capture generalized construction-related tendencies at the conceptual design stage. Accurate prediction of actual construction costs would require BIM quantities, fabrication records, labour productivity, supplier prices, contractor quotations, and erection records, which vary significantly across projects.

Accordingly, the present framework is positioned as a decision-support tool for early-stage structural design, where relative comparison among alternative configurations is more critical than precise cost quantification. Future work may focus on calibrating the proposed indices against real construction data, integrating project-specific parameters, and extending the methodology toward more detailed design and cost assessment scenarios.

CRediT authorship contribution statement

Yuan Ma: Writing – original draft, Visualization, Methodology, Formal analysis. **Chaolin Song:** Writing – review & editing, Methodology, Investigation. **Laura Sardone:** Writing – review & editing, Formal analysis. **Rucheng Xiao:** Supervision, Funding acquisition. **Giuseppe Carlo Marano:** Supervision, Resources.

Funding

This research was funded by National Natural Science Foundation of China, grant number 52308196. The first author acknowledges the support of the China Scholarship Council (202406260131) during his study at Politecnico di Torino. The opinions and statements do not necessarily represent those of the sponsors.

Declaration of competing interest

The authors declare that they have no known competing financial interests or personal relationships that could have appeared to influence the work reported in this paper.

Appendix A. Cross-section clustering

In all three case studies, topology and member sizing are optimized simultaneously. Since different topological configurations generally contain different numbers of physical members, a direct member-wise definition of cross-sectional areas would lead to a high-dimensional design space and, more importantly, to an inconsistent number of design variables across candidate topologies. To address this issue, a response-based clustering strategy is adopted.

For each candidate topology, the clusterable members are first assigned a uniform reference cross-section, and a preliminary finite-element analysis is carried out under the prescribed load case or reference load combination. The resulting axial-force responses are then used as clustering features. Both the sign and the magnitude of the axial force are considered, so that tension- and compression-dominated members are classified separately, while members with similar force levels are grouped into the same cluster. All members within one cluster share a common cross-sectional design variable.

This strategy is used throughout Cases 1–3, as illustrated in Fig. 16. In Cases 1 and 2, clustering is applied to all structural members. In Case 3, clustering is applied to the roof-truss members, whereas the

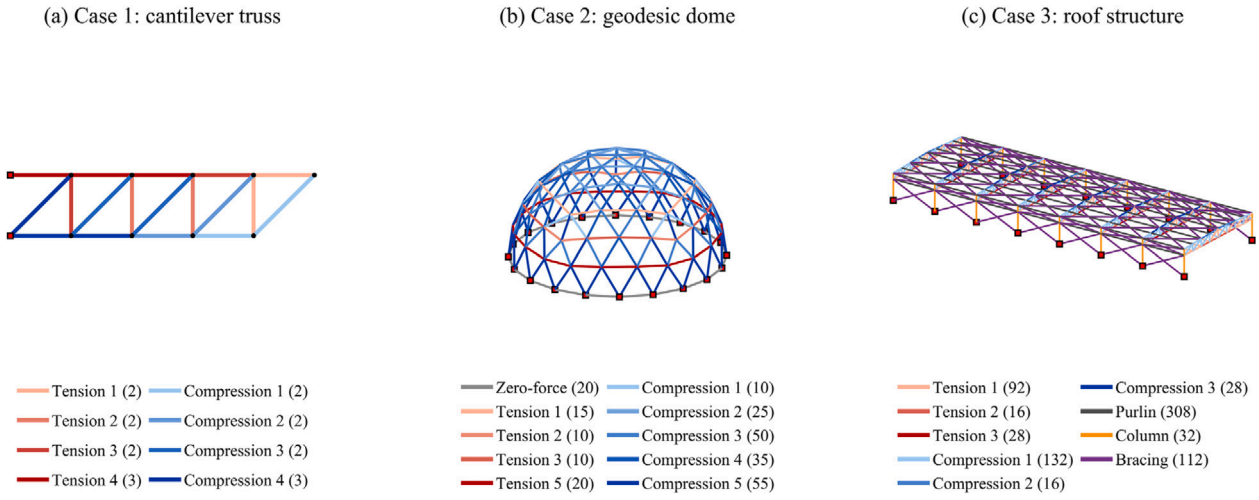

Fig. 16. Representative clustering results for the three case studies. Members are grouped according to the axial-force responses obtained from a preliminary finite-element analysis with uniform reference sections under the prescribed reference loading.

purlins, columns, and bracings are represented by separate sizing variables. In this way, the clustering strategy reduces the number of sizing variables and, more importantly, preserves a compact and consistent design-variable structure across different topological configurations.

Appendix B. Differentiable approximation

For problems involving continuous design variables, the availability of analytical derivatives can reduce computational costs and improve the efficiency and accuracy. To enable such gradient information, the cost model must be continuously differentiable with respect to the design variables. However, the typological complexity c_t and logistical complexity c_l, as originally defined in Section 2, involve discrete counting and non-differentiable max functions, respectively. These features prevent the use of gradient-based optimization methods. To address this, we introduce smooth approximations that render both cost components continuously differentiable with respect to the cross-sectional areas a_i, while preserving their essential physical and economic meanings.

B.1. Typological complexity: kernel density estimation

The exact calculation of profile multiplicity n_i, which underpins the typological complexity c_t, is inherently discrete:

$$n_i = \sum_{j=1}^{n_\mathrm{b}} \mathbf{1}(a_j = a_i), \tag{19}$$

where $\mathbf{1}(\cdot)$ is the indicator function:

$$\mathbf{1}(a_j = a_i) = \begin{cases} 1, & a_j = a_i \\ 0, & a_j \neq a_i \end{cases}. \tag{20}$$

This definition leads to a piecewise-constant and non-differentiable dependence of n_i on the design variables. To enable gradient computation, kernel density estimation (KDE) (Terrell & Scott, 1992) is employed to provide a smooth approximation of the discrete counting:

$$\tilde{n}_i = \sum_{j=1}^{n_\mathrm{b}} \exp\left(-\frac{(a_i - a_j)^2}{2h^2}\right), \tag{21}$$

where h is the bandwidth parameter (Chiu, 1991) controlling the smoothness. As $h \to 0$, the KDE estimate converges to the exact discrete multiplicity; in practice, h may be calibrated based on the spacing of available commercial profiles or fabrication tolerances. The price scaling factor γ_i is then computed using $\tilde{n}_i$ via the logistic function (Eq. (4)) introduced in Section 2.

B.2. Logistical complexity: softplus approximation

The logistical complexity c_l originally involves non-differentiable max functions through the penalty terms $\delta_{\mathrm{l},i}$ and $\delta_{\mathrm{w},i}$ (Eq. (9)). To enable gradient computation while preserving the threshold behavior, these terms are replaced with a smooth softplus approximation. For member i, define:

$$\begin{aligned} \tilde{\delta}_{\mathrm{l},i} &= \frac{1}{\kappa} \ln\left(1 + \mathrm{e}^{\kappa\left(\frac{l_i}{l_\mathrm{ref}} - 1\right)}\right), \\ \tilde{\delta}_{\mathrm{w},i} &= \frac{1}{\kappa} \ln\left(1 + \mathrm{e}^{\kappa\left(\frac{w_i}{w_\mathrm{ref}} - 1\right)}\right), \end{aligned} \tag{22}$$

where $\kappa > 0$ is a smoothness parameter; as $\kappa \to \infty$, these expressions converge to the original $\max(0, \cdot)$ functions.

With these modifications, both c_t and c_l, together with the already linear w_tot and c_n, become continuously differentiable with respect to all cross-sectional areas a_i. Fig. 17 plots the approximation functions and their derivatives.

Appendix C. Gradient derivation

Building upon the differentiable approximations established above, we now derive the analytical gradients of each cost component with respect to the cross-sectional areas a_i.

C.1. Gradient of structural weight w_{tot}

Since the structural weight w_tot is linear in each a_i, its partial derivative is straightforward:

$$\frac{\partial w_\mathrm{tot}}{\partial a_i} = \rho_\mathrm{stl} l_i. \tag{23}$$

C.2. Gradient of typological complexity c_t

The typological complexity c_t defined in Eq. (11) depends on a_i through both γ_j (via the KDE-smoothed multiplicities $\tilde{n}_j$ from Eq. (21)) and the relative weights r_j. Applying the chain rule:

$$\frac{\partial c_\mathrm{t}}{\partial a_i} = \sum_{j=1}^{n_\mathrm{b}} \left[\frac{\partial \gamma_j}{\partial \tilde{n}_j} \cdot \frac{\partial \tilde{n}_j}{\partial a_i} \cdot r_j + \gamma_j \cdot \frac{\partial r_j}{\partial a_i}\right]. \tag{24}$$

The derivative of the relative weight $r_j = w_j / w_\mathrm{tot}$ with respect to a_i is:

$$\frac{\partial r_j}{\partial a_i} = \begin{cases} \dfrac{\rho_\mathrm{stl} l_i}{w_\mathrm{tot}} \left(1 - r_i\right), & j = i \\ -\dfrac{\rho_\mathrm{stl} l_i}{w_\mathrm{tot}} r_j, & j \neq i \end{cases}. \tag{25}$$

The derivative of the logistic function (Eq. (4)) is:

$$\frac{\partial \gamma_j}{\partial \tilde{n}_j} = -\frac{(\gamma_\mathrm{max} - \gamma_\mathrm{min}) k \exp\left(k(\tilde{n}_j - n^*)\right)}{\left(1 + \exp\left(k(\tilde{n}_j - n^*)\right)\right)^2}. \tag{26}$$

The derivative of the KDE estimate (Eq. (21)) with respect to a_i is:

$$\frac{\partial \tilde{n}_j}{\partial a_i} = \begin{cases} \displaystyle\sum_{k \neq i} \frac{a_k - a_i}{h^2} \exp\left(-\frac{(a_i - a_k)^2}{2h^2}\right), & j = i \\ \dfrac{a_j - a_i}{h^2} \exp\left(-\dfrac{(a_j - a_i)^2}{2h^2}\right), & j \neq i \end{cases}. \tag{27}$$

C.3. Gradient of nodal complexity c_n

The nodal complexity c_n defined in Eq. (11) can be expressed as

$$c_\mathrm{n} = \sum_{i=1}^{n_\mathrm{b}} 2\, r_i \frac{l_\mathrm{c}}{l_i}, \tag{28}$$

since each member contributes to the node cost at its two end nodes. It depends on a_i through the relative weights r_j. Using the chain rule,

$$\frac{\partial c_\mathrm{n}}{\partial a_i} = \sum_{j=1}^{n_\mathrm{b}} 2 \frac{l_\mathrm{c}}{l_j} \frac{\partial r_j}{\partial a_i}. \tag{29}$$

Substituting $\partial r_j / \partial a_i$ from Eq. (25) and simplifying yields

$$\frac{\partial c_\mathrm{n}}{\partial a_i} = \frac{\rho_\mathrm{stl} l_i}{w_\mathrm{tot}} \left(\frac{2 l_\mathrm{c}}{l_i} - c_\mathrm{n}\right). \tag{30}$$

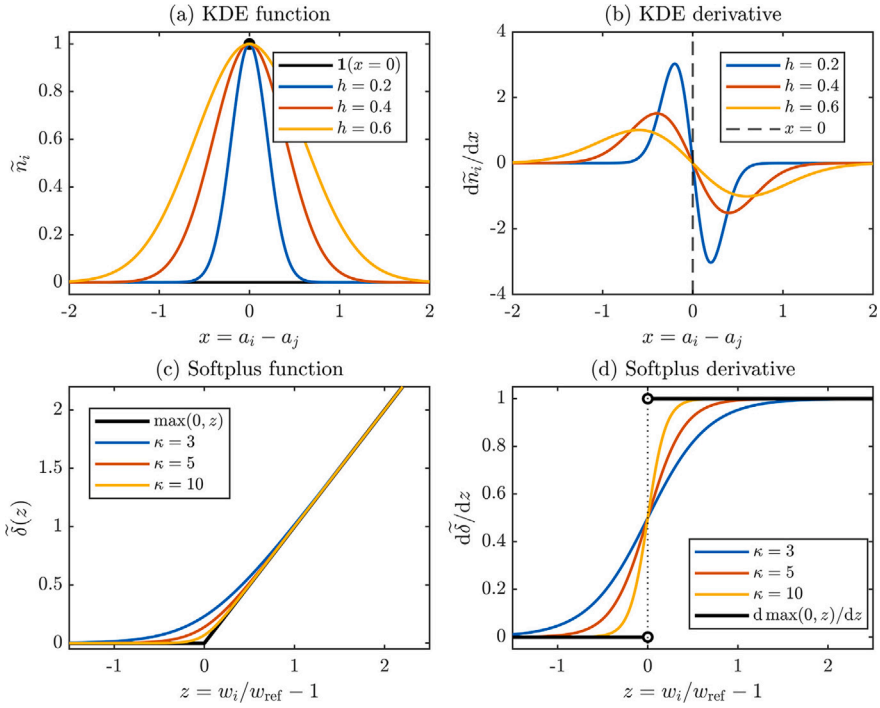

Fig. 17. Differentiable approximation functions: (a) KDE approximation function; (b) derivative of the KDE approximation; (c) Softplus approximation function; and (d) derivative of the Softplus approximation.

C.4. Gradient of logistical complexity c_l

The logistical complexity c_l defined in Eq. (11) incorporates the smooth approximations $\tilde{\delta}_{\mathrm{l},i}$ and $\tilde{\delta}_{\mathrm{w},i}$ introduced in Section B.2. Since l_i is constant, $\tilde{\delta}_{\mathrm{l},i}$ is independent of a_i, and its derivative vanishes. For $\tilde{\delta}_{\mathrm{w},i}$, using $w_i = \rho_{\mathrm{stl}} l_i a_i$, the derivative is:

$$\frac{\partial \tilde{\delta}_{\mathrm{w},i}}{\partial a_i} = \frac{1}{w_{\mathrm{ref}}} \cdot \frac{1}{1+\mathrm{e}^{-\kappa\left(\frac{w_i}{w_{\mathrm{ref}}}-1\right)}} \cdot \rho_{\mathrm{stl}} l_i. \tag{31}$$

Applying the chain rule and using $\partial r_j/\partial a_i$ from Eq. (25), the gradient of c_l is:

$$\frac{\partial c_\mathrm{l}}{\partial a_i} = \frac{p_{\log}}{p_{\mathrm{stl}}} \left[\left(1+\beta_\mathrm{l}\tilde{\delta}_{\mathrm{l},i}+\beta_\mathrm{w}\tilde{\delta}_{\mathrm{w},i}\right)\frac{\partial r_i}{\partial a_i} + \beta_\mathrm{w} r_i \frac{\partial \tilde{\delta}_{\mathrm{w},i}}{\partial a_i} + \sum_{j\neq i}\left(1+\beta_\mathrm{l}\tilde{\delta}_{\mathrm{l},j}+\beta_\mathrm{w}\tilde{\delta}_{\mathrm{w},j}\right)\frac{\partial r_j}{\partial a_i} \right]. \tag{32}$$

C.5. Verification and comparison

To evaluate the practical value of the analytical derivatives, a controlled continuous version of Case 1 (Section 3.1) is considered. The topology and geometry are fixed at $N_\mathrm{s} = 5$ and $H/L = 0.2$. The eight clustered cross-sectional areas remain continuous design variables. Since the structure is statically determinate and self-weight is omitted, the member forces are independent of the cross-sectional areas. Consequently, the stress constraints are expressed as area lower bounds and the weight constraint is linear, so that the comparison primarily reflects the treatment of the objective derivatives.

Three bi-objective problems are considered by minimizing the normalized structural weight $\bar{w} = w_{\mathrm{tot}}/w_{\mathrm{tot,ref}}$, together with c_t, c_n, or c_l. The gradient-based Pareto fronts are generated using the ε-constraint method (EC) (Haimes, 1971; Mavrotas, 2009), with each resulting continuous scalar problem solved by Sequential Quadratic Programming (SQP) (Nocedal & Wright, 1999). Two otherwise identical SQP implementations are compared: EC-SQP-ANA uses the analytical gradients derived in the preceding appendices, whereas EC-SQP-FD approximates the same derivatives using finite differences. Both implementations use identical weight budgets, initial designs, constraints, variable scaling, and stopping tolerances. NSGA-II (Deb et al., 2002) is applied to the same continuous problems as a derivative-free reference.

The results are shown in Fig. 18 and Table 11.

EC-SQP-ANA and EC-SQP-FD produce virtually identical Pareto fronts for all three complexity indices. This optimization-level agreement supports the correctness of the analytical derivatives. Compared with EC-SQP-FD, supplying the analytical gradients reduces the number of objective evaluations by approximately 70.8%, 75.5%, and 76.0% for c_t, c_n, and c_l, respectively. The corresponding computational times are reduced by approximately 35.4%, 14.1%, and 38.8%.

The analytical gradient-based method also obtains comparable or higher hypervolume values than NSGA-II with substantially fewer objective evaluations. NSGA-II nevertheless returns a denser set of non-dominated solutions because its population-based search generates multiple Pareto solutions concurrently (Deb et al., 2002). More importantly, the complete case studies in the main text contain discrete topological and cross-sectional decisions, for which derivatives with respect to the continuous member properties alone are insufficient. NSGA-II is therefore retained as the principal optimizer for the complete mixed-discrete problems, whereas the analytical framework provides an efficient basis for continuous subproblems, local refinement, and future hybrid global–local optimization procedures.

All computations were performed in MATLAB R2024a on a personal laptop equipped with an i9-14900HX processor and 16 GB of memory. The reported values are wall-clock times for a single serial run.

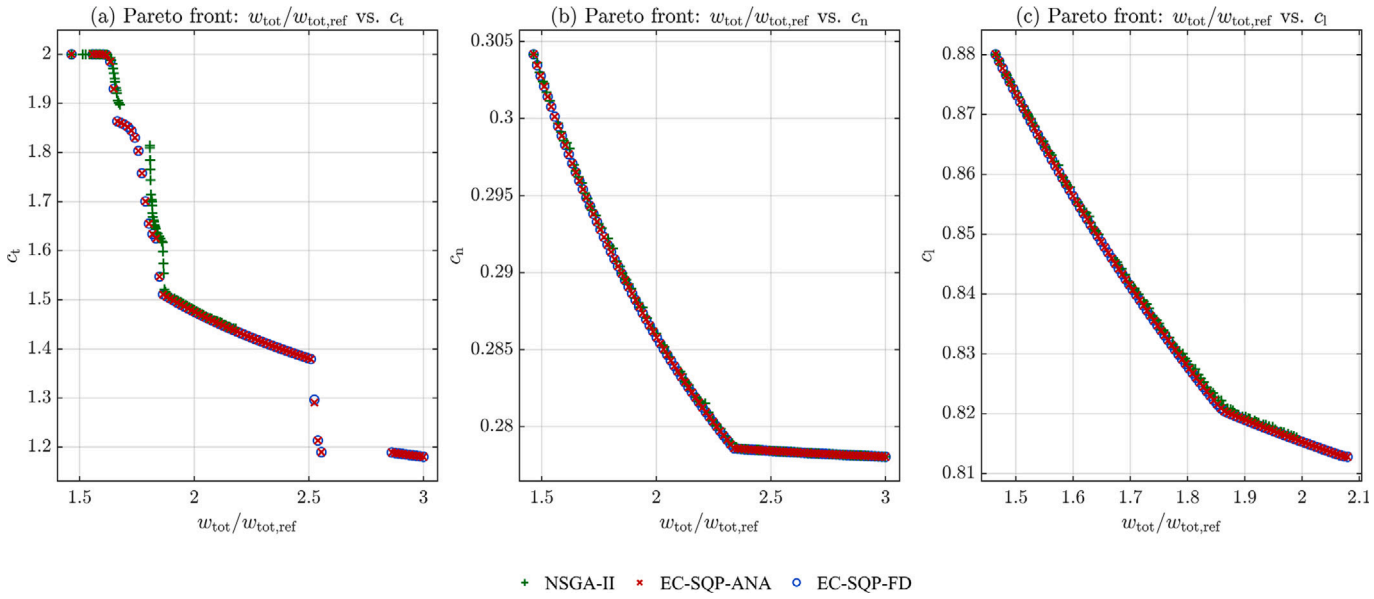

Fig. 18. Pareto fronts obtained using NSGA-II, analytical-gradient SQP (EC-SQP-ANA), and finite-difference SQP (EC-SQP-FD) for: (a) $\bar{w}$–c_t; (b) $\bar{w}$–c_n; and (c) $\bar{w}$–c_l.

Table 11
Comparison of NSGA-II and the gradient-based multi-objective procedures for the continuous Case 1 subproblem. The hypervolume indicator (Zitzler & Thiele, 1999) is evaluated after a common normalization of the combined non-dominated solutions.

Objective pair	Method	N_{PF}	Hypervolume	Objective evaluations	Solver time (s)
$\bar{w}$–c_t	NSGA-II	97	0.6097	46,800	33.16
	EC-SQP-ANA	78	0.7422	22,862	1.67
	EC-SQP-FD	78	0.7421	78,382	2.58
$\bar{w}$–c_n	NSGA-II	104	0.8415	32,700	32.60
	EC-SQP-ANA	101	0.8462	3074	0.42
	EC-SQP-FD	101	0.8462	12,549	0.49
$\bar{w}$–c_l	NSGA-II	104	0.7284	31,800	32.71
	EC-SQP-ANA	101	0.7423	12,295	0.83
	EC-SQP-FD	101	0.7423	51,311	1.35

Data availability

Data will be made available upon request.

References

An, J., Park, J. S., & Park, H. S. (2025). Integrated truss optimization using a ternary-quantized gradient method with implicit topology control. *Computer-Aided Civil and Infrastructure Engineering*, *40*, 6437–6455.

Arditi, D., Elhassan, A., & Toklu, Y. C. (2002). Constructability analysis in the design firm. *Journal of Construction Engineering and Management*, *128*, 117–126.

Asadpoure, A., Guest, J. K., & Valdevit, L. (2015). Incorporating fabrication cost into topology optimization of discrete structures and lattices. *Structural and Multidisciplinary Optimization*, *51*, 385–396.

Ashworth, A., & Skitmore, R. M. (1983). *The effectiveness of estimating in the construction industry*. Englemere, Berkshire, UK: The Chartered Institute of Building.

Azad, S. K., Aminbakhsh, S., & Shaban, S. S. (2021). Multi-stage guided stochastic search for optimization and standardization of free-form steel double-layer grids. In *Structures* (pp. 678–699). Elsevier.

Barg, S., Flager, F., & Fischer, M. (2018). An analytical method to estimate the total installed cost of structural steel building frames during early design. *Journal of Building Engineering*, *15*, 41–50.

Biedermann, J., & Grierson, D. (1995). A generic model for building design. *Engineering with Computers*, *11*, 173–184.

Carter, C. J., & Schlafly, T. J. (2008). $ave more money. Modern Steel Construction Smart design and detailing can add up to big savings in the total cost of fabricated structural steel.

Carvalho, J. P. G., Vargas, D. E., Jacob, B. P., Lima, B. S., Hallak, P. H., & Lemonge, A. C. (2024). Multi-objective structural optimization for the automatic member grouping of truss structures using evolutionary algorithms. *Computers & Structures*, *292*, 107230.

Chen, M. T., Zuo, W., Chen, Y., Zhao, O., Cheng, B., & Zhao, J. (2024). Parametric topology optimization design and analysis of additively manufactured joints in spatial grid structures. *Engineering Structures*, *300*, 117123.

Chiu, S. T. (1991). Bandwidth selection for kernel density estimation. *The Annals of Statistics*, 1883–1905.

Cucuzza, R., Aloisio, A., Rad, M. M., & Domaneschi, M. (2024). Constructability-based design approach for steel structures: From truss beams to real-world inspired industrial buildings. *Automation in Construction*, *166*, 105630.

De Biagi, V., Reggio, A., Rosso, M. M., & Sardone, L. (2024). Nondimensional shape optimization of nonprismatic beams with sinusoidal lateral profile. *Journal of Structural Engineering (ASCE)*, *150*.

Deb, K., Pratap, A., Agarwal, S., & Meyarivan, T. (2002). A fast and elitist multiobjective genetic algorithm: NSGA-II. *IEEE Transactions on Evolutionary Computation*, *6*, 182–197.

Dorn, W. S., Gomory, R. E., & Greenberg, H. J. (1964). Automatic design of optimal structures. *Journal de Mecanique*, *3*, 25–52.

Erbatur, F., & Al-Hussainy, M. (1992). Optimum design of frames. *Computers & Structures*, *45*, 887–891.

European Committee for Standardization. (2005). *EN 1993-1-1: Eurocode 3: Design of steel Structures—Part 1-1: General rules and rules for buildings*.

Evers, H., & Maatje, I. (2000). Cost based engineering and production of steel constructions. In *Steel design codes—fourth international workshop on connections in steel structures* (pp. 14–22). American Society of Civil Engineering (ASCE) Fort Collins, CO, USA.

Frangedaki, E., Sardone, L., & Lagaros, N. D. (2021). Design optimization of tree-shaped structural systems and sustainable architecture using bamboo and earthen materials. *Journal of Architectural Engineering*, *27*.

Haimes, Y. (1971). On a bicriterion formulation of the problems of integrated system identification and system optimization. *IEEE Transactions on Systems, Man, and Cybernetics*, 296–297.

Havelia, P. (2016). *A ground structure method to optimize topology and sizing of steel frame structures to minimize material, fabrication and erection cost* (Master's thesis). Stanford University.

Hayalioglu, M., & Degertekin, S. (2005). Minimum cost design of steel frames with semi-rigid connections and column bases via genetic optimization. *Computers & Structures*, *83*, 1849–1863.

He, L., & Gilbert, M. (2015). Rationalization of trusses generated via layout optimization. *Structural and Multidisciplinary Optimization*, *52*, 677–694.

Holland, J. H. (1992). Genetic algorithms. *Scientific American*, *267*, 66–73.

Hu, X., Lu, M., & AbouRizk, S. M. (2014). BIM-based data mining approach to estimating job man-hour requirements in structural steel fabrication. In *Proceedings of the 2014 winter simulation conference* (pp. 3399–3410). IEEE.

Jármai, K., & Farkas, J. (1999). Cost calculation and optimisation of welded steel structures. *Journal of Constructional Steel Research*, *50*, 115–135.

Karadimos, P., & Anthopoulos, L. (2024). A taxonomy of machine learning techniques for construction cost estimation. *Innovative Infrastructure Solutions*, *9*, 420.

Kociecki, M., & Adeli, H. (2015). Shape optimization of free-form steel space-frame roof structures with complex geometries using evolutionary computing. *Engineering Applications of Artificial Intelligence*, *38*, 168–182.

Krishnamoorthy, C., Prasanna Venkatesh, P., & Sudarshan, R. (2002). Object-oriented framework for genetic algorithms with application to space truss optimization. *Journal of Computing in Civil Engineering*, *16*, 66–75.

Laghi, V., Babovic, N., Benvenuti, E., & Kloft, H. (2024). Blended structural optimization of steel joints for wire-and-arc additive manufacturing. *Engineering Structures*, *300*, 117141.

Lai, Y., Cai, Q., Li, Y., Chen, J., & Xie, Y. M. (2025). A new evolutionary topology optimization method for truss structures towards practical design applications. *Engineering Structures*, *324*, 119326.

Liu, Y., Lee, T. U., Koronaki, A., Pietroni, N., & Xie, Y. M. (2023). Reducing the number of different nodes in space frame structures through clustering and optimization. *Engineering Structures*, *284*, 116016.

Lu, H., & Xie, Y. M. (2023). Reducing the number of different members in truss layout optimization. *Structural and Multidisciplinary Optimization*, *66*, 52.

Ma, Y., Song, C., Sardone, L., Xiao, R., & Marano, G. C. (2026). Surrogate-assisted design optimization of cable-stayed bridges with dynamic trust threshold-based active learning. *Structural and Multidisciplinary Optimization*, *69*, 97.

Mavrotas, G. (2009). Effective implementation of the ε-constraint method in multi-objective mathematical programming problems. *Applied Mathematics and Computation*, *213*, 455–465.

Melchiorre, J., Manuello Bertetto, A., Adriaenssens, S., & Marano, G. C. (2025). Form-finding and metaheuristic multiobjective optimization methodology for sustainable gridshells with reduced construction complexity and waste. *Automation in Construction*, *177*, 106315.

Melchiorre, J., Manuello Bertetto, A., Marano, G. C., & Adriaenssens, S. (2026). AI-driven human-in-the-loop structural optimization of gridshells. *Computer-Aided Civil and Infrastructure Engineering*, *49*, 100044.

Mohsenijam, A., & Lu, M. (2016). Achieving sustainable structural steel design by estimating fabrication labor cost based on BIM data. *Procedia Engineering*, *145*, 654–661.

Moroni, G., & Forcael, E. (2026). Balancing performance and constructability: A multi-objective optimization framework for low-carbon 2D truss design. *Structures*, *87*, 111705.

Nocedal, J., & Wright, S. J. (1999). *Numerical optimization*. New York, NY, USA: Springer.

Ouda, E., & Haggag, M. (2025). Cost-benefit analysis of automating modular construction manufacturing for affordable housing. *Frontiers in Built Environment*, *11*, 1713686.

Parkes, E. (1975). Joints in optimum frameworks. *International Journal of Solids and Structures*, *11*, 1017–1022.

Pavlovčič, L., Krajnc, A., & Beg, D. (2004). Cost function analysis in the structural optimization of steel frames. *Structural and Multidisciplinary Optimization*, *28*, 286–295.

Peng, J., Feng, Y., Zhang, Q., & Liu, X. (2023). Multi-objective integrated optimization study of prefabricated building projects introducing sustainable levels. *Scientific Reports*, *13*, 2821.

Pishdad, P., & Onungwa, I. O. (2024). Analysis of 5D BIM for cost estimation, cost control and payments. *Journal of Information Technology in Construction*, *29*, 525–548.

Rafiei, M. H., & Adeli, H. (2018). Novel machine-learning model for estimating construction costs considering economic variables and indexes. *Journal of Construction Engineering and Management*, *144*, 04018106.

Rajeev, S., & Krishnamoorthy, C. (1992). Discrete optimization of structures using genetic algorithms. *Journal of Structural Engineering*, *118*, 1233–1250.

Ranalli, F., Flager, F., & Fischer, M. (2018). A ground structure method to minimize the total installed cost of steel frame structures. *World Acad. Sci. Eng. Technol. Int. J. Civ. Environ. Eng*, *12*, 115–123.

Ruby, D. I. (2008). *Constructability of structural steel buildings*. AISC Steel Design Guide No. 23. Chicago, IL, USA: American Institute of Steel Construction.

Russell, J. S., Swiggum, K. E., Shapiro, J. M., & Alaydrus, A. F. (1994). Constructability related to TQM, value engineering, and Cost/Benefits. *Journal of Performance of Constructed Facilities*, *8*, 31–45.

Ruy, W. S., Yang, Y. S., Kim, G. H., & Yeun, Y. S. (2001). Topology design of truss structures in a multicriteria environment. *Computer-Aided Civil and Infrastructure Engineering*, *16*, 246–258.

Saif, W., RazaviAlavi, S., & Kassem, M. (2024). Construction digital twin: A taxonomy and analysis of the application-technology-data triad. *Automation in Construction*, *167*, 105715.

Sarma, K. C., & Adeli, H. (2000). Cost optimization of steel structures. *Engineering Optimization*, *32*, 777–802.

Sirca Jr, G. F., & Adeli, H. (2005). Cost optimization of prestressed concrete bridges. *Journal of Structural Engineering*, *131*, 380–388.

Soh, M. F., Bigras, D., Barbeau, D., Doré, S., & Forgues, D. (2022). BIM machine learning and design rules to improve the assembly time in steel construction projects. *Sustainability*, *14*, 288.

SteelConstruction.info. (2024). *Cost of structural steelwork*. https://steelconstruction.info/Cost_of_structural_steelwork.

Stigler, G. J. (1958). The economies of scale. *The Journal of Law and Economics*, *1*, 54–71.

Terrell, G. R., & Scott, D. W. (1992). Variable kernel density estimation. *The Annals of Statistics*, 1236–1265.

Torii, A. J., Lopez, R. H., & Miguel, L. F. F. (2016). Design complexity control in truss optimization. *Structural and Multidisciplinary Optimization*, *54*, 289–299.

Van Mellaert, R., Lombaert, G., & Schevenels, M. (2016). Global size optimization of statically determinate trusses considering displacement, member, and joint constraints. *Journal of Structural Engineering*, *142*, 04015120.

van Woudenberg, T. R., & van Der Meer, F. P. (2021). A grouping method for optimization of steel skeletal structures by applying a combinatorial search algorithm based on a fully stressed design. *Engineering Structures*, *249*, 113299.

Vares, S., Hradil, P., Sansom, M., Ungureanu, V., & Kamrath, P. (2019). *Economic assessment of reusing steel-based elements*. Deliverable D5.2 RFCS Grant Agreement No. 747847. PROGRESS project: Provisions for Greater Reuse of Steel Structures, VTT Technical Research Centre of Finland.

Walls, R., & Elvin, A. (2010). An algorithm for grouping members in a structure. *Engineering Structures*, *32*, 1760–1768.

Zawidzki, M., & Jankowski, Ł. (2019). Multiobjective optimization of modular structures: Weight versus geometric versatility in a truss-Z system. *Computer-Aided Civil and Infrastructure Engineering*, *34*, 1026–1040.

Zhang, X., Xie, Y. M., & Zhou, S. (2023). A nodal-based evolutionary optimization algorithm for frame structures. *Computer-Aided Civil and Infrastructure Engineering*, *38*, 288–306.

Zitzler, E., & Thiele, L. (1999). Multiobjective evolutionary algorithms: A comparative case study and the strength Pareto approach. *IEEE Transactions on Evolutionary Computation*, *3*, 257–271.